eGFP-Tagging of the Dopamine D2 Receptor: Re-examination of Subcellular Receptor Localization in the Substantia Nigra and Dorsolateral Striatum of Transgenic Mice

by

Mason Alexander Trinkle

Neuroscience, Bachelor of Philosophy, University of Pittsburgh, 2019

Submitted to the Graduate Faculty of

University Honors College in partial fulfillment

of the requirements for the degree of

Bachelor of Philosophy

University of Pittsburgh

2019

UNIVERSITY OF PITTSBURGH

UNIVERSITY HONORS COLLEGE

This thesis was presented

by

Mason Alexander Trinkle

It was defended on

March 25, 2019

and approved by

Kevin Bender, Ph.D., Department of Neurology, University of California, San Francisco

Stephen D. Meriney, Ph.D., Department of Neuroscience, University of Pittsburgh

Maria E. Rubio, M.D., Ph.D., Department of Neurobiology, University of Pittsburgh School of Medicine

Thesis Advisor: Susan R. Sesack, Ph.D., Department of Neuroscience, University of Pittsburgh

eGFP-Tagging of the Dopamine D2 Receptor: Re-examination of Subcellular Receptor Localization in the Substantia Nigra and Dorsolateral Striatum of Transgenic Mice

Mason Alexander Trinkle, BPhil

University of Pittsburgh, 2019

The release of dopamine (DA) in the dorsal striatum modulates response to cortical input, facilitating fine motor skill planning and goal-directed behaviors. The neurons producing this DA signal originate in the midbrain substantia nigra pars compacta (SNc), where they autoregulate by releasing DA from their soma and dendrites onto D2-type autoreceptors (D2R) of neighboring cells. Exactly how DA transmits through the extracellular space, however, is not fully understood. Electrophysiological evidence suggests that DA release and receipt must be in close proximity to each other, possibly involving non-traditional synapses. This study sought to test for anatomical evidence supporting close proximity of D2Rs to dendrites that could transmit DA in the SNc.

Brain tissue from a transgenic mouse strain possessing a knock-in of enhanced green fluorescent protein (eGFP) on the D2R was labeled with immunogold antibodies directed against eGFP. This immunogold labeling was then analyzed by electron microscopy to determine the subcellular distribution of the D2R. Image analysis showed that in dendrites and axon terminals of the SNc, eGFP-D2R immunogold was found more often intracellularly than along the membrane. Intracellular immunogold was most often associated with the smooth endoplasmic reticulum, where it likely represents a transport form of D2R. Distal dendrites contained proportionally more immunogold on the plasma membrane suggesting specialized DA receipt sites. Immunogold for eGFP-D2R was also found at rare dendrodendritic synapses. Throughout all profiles in the SNc, eGFP-D2R immunogold particles were randomly spread along the membrane and rarely (7%)

directly apposed to other dendrites. In a comparative study of the dorsolateral striatum in the same animals, both total and membrane-bound eGFP-D2R were significantly higher than in the SNc and more frequently apposed to dendrites. These results indicate that the findings in the SNc were not unduly affected by methodology. Furthermore, the outcomes are more consistent with volume transmission serving intercellular DA communication in the SNc than non-traditional synapses. A novel discovery was also made that D2Rs are present on the axon initial segments of SNc neurons. These may serve a potent autoregulatory function that has yet to be physiologically defined for DA cells.

Table of Contents

List of Tables

List of Figures

Preface

I would first like to profusely thank my parents, James and Kimberly Trinkle, along with all of my grandparents for their blind and unwavering support of me throughout the process of completing this project.

My sincerest gratitude is extended to my professor and mentor, Dr. Susan R. Sesack, for the guidance that she has provided me over the past two years. I cannot thank her enough for the countless hours and valuable energy that she has invested into my personal and academic growth. I greatly appreciated her skillful abilities as a teacher and advisor, which have helped me every step of the way. Throughout my time in the lab, she has always ensured that I felt competent and that I believed that my contributions were significant. It has been a true pleasure every time that we worked together, and her presence has had a momentous and consistently-positive impact on my life.

I would also like to thank the research assistant and my teacher Judith Joyce Balcita-Pedicino, who instructed me on the countless difficult benchtop procedures that she has mastered. She has always been a caring and wholesome influence on my experience in the lab.

I would like to extend additional gratitude to my former fellow research assistant Savas Hetelekides for his hard work and thoughtful analysis in the beginning stages of this project, along with the helpful instruction that he provided me when I began in the lab.

Finally, I would like to thank my defense committee members, Dr. Kevin Bender, Dr. Lania Rubio, and Dr. Stephen Meriney, for taking time out of their busy schedules to positively challenge my critical thinking and help me showcase the scientific skills that I have acquired during my four years at Pitt.

List of Abbreviations

AIS	Axon initial segment
D1R	Dopamine receptor (type 1)
D2R	Dopamine receptor (type 2)
DA	Dopamine
eGFP	Enhanced green fluorescent protein
GABA	Gamma-Aminobutyric acid
GIRK	G-protein coupled inwardly-rectifying potassium channel
GP	Globus pallidus
MSN	Medium spiny neuron
MV body	Multivesicular body
NAc	Nucleus accumbens
NMDA	N-Methyl-D-aspartic acid
Ser	Smooth endoplasmic reticulum
SNc	Substantia nigra pars compacta
SNr	Substantia nigra pars reticulata
Str	Striatum
VMAT2	Vesicular monoamine transporter-2
VTA	Ventral tegmental area

1.0 Introduction

Dopamine (DA) is a neuronal signaling molecule that contributes to a number of important behaviors, and dysfunction in DA brain systems produces symptoms in multiple clinical diseases. The deterioration of DA brain levels found in patients with Parkinson's disease was one of the first observations that helped Arvid Carlsson define DA's neurotransmitter role and provided insight into its influence on motor control (Borroto-Escuela et al 2018, Fahn 2015). Other disruptions in DA neurotransmission have subsequently been associated with substance abuse disorder, depression, schizophrenia, and attention deficit hyperactivity disorder (Dunlop & Nemeroff 2007, Grace 2016, Kollins & Adcock 2014, McCutcheon et al 2019, Solinas et al 2018, Volkow et al 2017). These associations helped to confirm DA's fundamental roles in regulating cognition, learning, and goal-directed behaviors by adjusting various forebrain control systems. On the whole, the influence of DA enriches the signals being processed in different areas of the brain, allowing for more complex functioning than possible without this key modulator.

The exact functional implications of DA's actions depend on the specific area of the brain being targeted. For example, the largest and best-known dopaminergic system is the nigrostriatal pathway. The neurons comprising this projection originate in the substantia nigra pars compacta (SNc) of the midbrain and project to the striatum (Str), which in rodents includes an intermixed caudate and putamen within the basal ganglia complex (Fallon & Loughlin 1995). Because of the Str's role in adaptive motor control, DA has a significant influence on the facilitation of fine motor skills (David et al 2005). Additional projections, the DA mesocortical and mesolimbic pathways, innervate, respectively, the prefrontal cortex and the ventral striatum (also known as the nucleus accumbens; NAc), enabling them to regulate cognitive functioning and goal-directed behaviors

(Gentry et al 2018, Sesack & Grace 2010). The DA neurons comprising these pathways originate in the ventral tegmental area (VTA) located medial to the SNc.

1.1 Physiology of Dopamine's Actions in Target Regions

Within its target areas, DA does not strictly act as a neurotransmitter, which would directly influence membrane potential and, therefore, firing rate. Instead, it functions as a neuromodulator, in that the release of DA onto a neuron influences how the cell will respond to its other chemical signals. For example, DA modulation can either attenuate or potentiate a neuron's response to an excitatory stimulus. In the case of the dorsal Str, glutamatergic neurons from the motor cortex act as the dominant excitatory stimulus for medium spiny neurons (MSN), which comprise the bulk of cells in this region (Smith & Bolam 1990). Stimulations of the corresponding DA neurons in the SNc 100 ms before cortical stimulation can either attenuate or enhance the excitatory response of MSNs to subsequent cortical activation (Hirata et al 1984). A similar effect has also been shown in the mesolimbic pathway, where stimulation of VTA DA neurons influences the sensitivity of cells in the NAc to excitatory inputs (Ikemoto 2007, Sesack & Grace 2010). More specifically, repetitive stimulation of the VTA attenuates the response of cells in the NAc to both amygdala and hippocampal stimulation (Yang & Mogenson 1984, Yim & Mogenson 1982). In the third major dopaminergic pathway, the response of the medial prefrontal cortex to excitatory signaling from the mediodorsal nucleus of the thalamus can be reduced by prior stimulation of the VTA (Ferron et al 1984). Hence, DA's influence on different brain areas is both specific and varied, although its effects frequently involve modulation of excitatory glutamate transmission from different sources.

The specific direction of DA modulation on target neurons depends primarily on the subtype of DA receptors expressed. There are five known subtypes of G-protein coupled DA receptors, grouped into two receptor families: D1-like (D1 and D5) and D2-like (D2, D3, and D4) (Missale et al 1998). In the Str, DA's ability to facilitate cortical glutamate excitation is mediated mainly through D1 receptors, whereas its ability to attenuate corticostriatal transmission is primarily through D2 receptors located on the MSNs (Vives & Mogenson 1986). The attenuating effects of DA can also be achieved by targeting presynaptic axon terminals. For example, D2 receptors located on hippocampal terminals in the NAc reduce quantal release of excitatory neurotransmitters, which further attenuates corticostriatal transmission (Yang & Mogenson 1986). The different subtypes of DA receptors also work through separate mechanisms of glutamate receptor modulation. Activation of D1 receptors on MSNs potentiates neuronal excitability through modulation of NMDA currents, whereas activation of D2 receptors attenuates excitability by regulating both NMDA and non-NMDA currents (Cepeda et al 1993).

1.2 SNc DA Anatomy

Of the three main dopaminergic pathways originating from the midbrain, this paper will focus on the DA neurons of the nigrostriatal pathway. This population was chosen because the DA cells comprise roughly 95% of the tract (Rodriguez & Gonzalez-Hernandez 1999, van der Kooy et al 1981), contrasting the greater heterogeneity of neurons in the VTA (Li et al 2013, Nair-Roberts et al 2008). DA cells have pyramidal or polygonal shaped somas, 12-30 μm in diameter. Within the SNc, they commonly have 3 to 6 major dendrites, 4-8 μm in diameter, some of which can extend ventrally into the substantia nigra pars reticulata (SNr). A thin axon, less than 1 μm in

diameter, will commonly branch off of a major dendrite 10-70 µm from the soma and taper rapidly (Gonzalez-Cabrera et al 2017, Grace & Bunney 1983b, Meza et al 2018). The majority of these axons project to the dorsal Str, where they exhibit extensive arborization (Matsuda et al 2009) and synapse onto multiple GABAergic MSNs (Gauthier et al 1999, Pickel et al 1988). MSNs compose the bulk of striatal neurons, are of medium size, and have dendrites densely covered with spines (Smith & Bolam 1990). MSNs receive mainly excitatory input from the sensorimotor cortex, the axon terminals of which synapse onto the heads of dendritic spines. Dopaminergic terminals from the SNc then synapse onto the neck of these same spines, forming a triad of neural processes (Bouyer et al 1984, Dube et al 1988, Smith & Bolam 1990). This close proximity between DA release and extrinsic glutamate input on the MSNs allows DA to precisely modulate how individual spines react to cortical excitation (Nakano et al 2013).

1.3 Physiology of SNc Dopamine Neurons

Along with their specialized morphology, DA neurons possess multiple distinctive physiological characteristics. The main firing pattern of SNc DA neurons is comprised of tonic, single-spike, long duration (2-4 ms), action potentials that are preceded by slow and repetitive depolarization. The tonic firing rate is usually 3 to 7 Hz, as shown in electrophysiological recording from anesthetized or freely-moving animals and brain slices (Grace & Bunney 1983c, Lammel et al 2008, Steinfels et al 1981). Separate from this tonic activity is spontaneous bursting, characterized by rapid successions of up to 24 spikes, with each spike progressively decreasing in amplitude and increasing in duration and inter-spike interval (Grace & Bunney 1983a).

Some characteristics of SNc DA cell activity are only detectable in freely-moving animals, as opposed to anesthetized animals or brain slices. For example, recording of neurons in freely-moving cats (Steinfels et al 1981) were able to confirm that single DA cells can display both slow tonic firing and fast burst firing, whereas these two activities were only recorded independently in anesthetized animals (Grace & Bunney 1983a, Steinfels et al 1981), and it has been challenging to observe natural bursts in vitro (Shepard & Bunney 1988). Research using freely-moving animals has also reported synchronous firing between neighboring DA neurons, suggesting electronic coupling that is less noticeable in paralyzed or anesthetized rats (Freeman et al 1985, Grace & Bunney 1983c). Such differences between *in vitro*, *in vivo* anesthetized, and *in vivo* freely-moving recordings introduced some doubt about the validity of early DA neuron identification methods. Collaborative analysis of these studies, however, has shown that the criteria used for identifying DA neurons in anesthetized animals is comparable to that used in modern studies using other preparations (Ungless & Grace 2012).

As noted above, SNc DA neurons do not exhibit natural burst firing when recorded in brain slices (Grace 1990, Shepard & Bunney 1988). The most conservative explanation of this observation is that extrinsic inputs not included in the plane of slices must be necessary to induce bursting. The SNc receives excitatory glutamatergic afferents from the somatosensory/motor cortices, subthalamic nucleus, pedunculopontine nucleus, and the lateral habenula (Kitai et al 1999, Watabe-Uchida et al 2012, Zahm & Root 2017). These excitatory inputs provide depolarizing factors that spur burst firing in the SNc. Another significant factor in determining burst firing is the degree of GABAergic tone exerted onto DA cells, and inhibitory inputs from the substantia nigra reticulata (SNr), rostromedial mesopontine tegmental nucleus, globus pallidus (GP), and Str provide such tone (Bourdy et al 2014, Kitai et al 1999, Tepper et al 1995, Yetnikoff

et al 2014). Constant inhibition may gate DA neurons' burst firing, countering active excitatory drive, such that blocking GABA(A) receptors in the SNc could substantially increase burst firing (Paladini & Tepper 1999). An example of this disinhibitory mechanism is demonstrated by the burst firing that occurs when the GP is stimulated. Projections from the GP inhibit tonic GABAergic influence from neurons of the SNr, consequently removing inhibition from the SNc (Celada et al 1999). Even more complex networks can have an impact on the balance of inhibition and excitation of SNc DA neurons, some even relying on the activity of DA cells themselves. For example, transgenic mice whose SNc neurons are prevented from synthesizing and storing DA show burst firing only when L-DOPA is administered systemically. This finding suggests that the nigral release of DA in one of its target areas likely has an effect on burst firing in the SNc through a network feedback mechanism (Paladini et al 2003).

Burst firing is essential to the transmission of information from the SNc to target areas. Action potential bursts releases more DA in the Str than the same number of spikes fired at a tonic pace (Floresco et al 2003, Gonon & Buda 1985, Lohani et al 2018). This dramatic difference in release efficiency enables the firing of DA neurons to transmit a variety of messages to Str cells, which is especially valuable when modulating the basal ganglia's response to rewarding stimuli. In the awake behaving monkey, SNc DA cells have been shown to fire phasically in bursts when a novel reward is presented. If this reward is anticipated, however, DA neuron firing remains tonic, and the reward elicits no burst (Schultz 1998). The significance of this phenomenon has been explained by a theory of reward prediction error, in which the purpose of reward-induced DA bursting is to differentiate between a reward and its prediction. The increased DA release in the dorsal Str from bursting is likely to strengthen the synapses responsible for the behavior that

produced the reward (Montague et al 1996). Hence, bursting is a firing pattern through which midbrain DA neurons facilitate the repetition of beneficial actions.

Separate from burst firing, DA neurons can also exhibit transient periods of depressed firing. This drop in activity and consequent striatal DA release is yet another distinct response of midbrain DA cells that can occur, for example, when an anticipated reward is suddenly omitted (Schultz 1998). The deviation from normally tonic DA release in the Str likely weakens connections associated with actions that are no longer being rewarded (Montague et al 1996). This RPE theory (Gentry et al 2018, Keiflin & Janak 2015, Montague et al 1996, Schultz 1998) explains a possible neural mechanism supporting goal-directed behavior as well as the likely behavioral significance of tonic DA firing, phasic DA bursts, and sudden, brief periods of depressed activity.

1.4 Autoinhibition in the SNc

Given the importance of midbrain DA cell firing rates and patterns for reward learning, it is essential to understand how this system self-governs. One of the largest regulators of DA cell firing is autoinhibition activated at somatodendritic sites in the SNc. The exact mechanism by which DA is released from these sites is not yet understood (see section below), but it is known that the inhibitory response is mediated solely by D2 autoreceptors (D2R) (Beckstead et al 2004, Ford 2014, Mercuri et al 1997, Morelli et al 1988). An early light and electron microscopic immunocytochemical study in the SNc revealed the presence of this receptor on soma, proximal dendrites, and distal dendrites of identified DA neurons, specifically localized to saccules of smooth endoplasmic reticulum (ser) as well as along synaptic- and non-synaptic sections of the plasma membrane (Sesack et al 1994).

D2Rs modulate DA cell activity through activating G-protein coupled, inhibitory inwardly-rectifying potassium (GIRK) channels. Activated GIRK channels evoke inhibitory post synaptic currents (IPSCs) that reduce both cell excitability and firing rate (Williams & Lacey 1988). These inhibitory responses to DA are blocked by the presence of D2R antagonists (Beckstead et al 2004).

The effect of D2R autoinhibition is especially influential on further somatodendritic DA release, in part because the axon often branches off a major dendrite instead of directly off the soma. This arrangement causes a larger percentage of action potentials to fail when backpropagating from the axon-bearing dendrite into the somatodendritic complex (Gentet & Williams 2007). The presence of DA exacerbates this failure by activating D2Rs and creating a subsequent membrane hyperpolarization. In this way, DA released locally within the SNc reduces action potential frequency as well as action potential-dependent somatodendritic DA release by decreasing the probability of action potentials backpropagating into and through the somatodendritic complex. By gating compartmental cell firing, D2R autoinhibition can affect both somatodendritic as well as axonal DA release (Gentet & Williams 2007). This mechanism joins traditional D2R-IPSC mediated inhibition of action potential generation as a means for autoreceptors to indirectly affect DA neurotransmission (Williams & Lacey 1988).

A direct inhibition of somatodendritic release, independent from impulse control, is also mediated by D2R autoreceptors, although the cellular mechanism for release modulation is not well understood (Cragg & Greenfield 1997). Additionally, activation of D2Rs decreases the rate of DA synthesis by decreasing cyclic AMP levels, resulting in lowered phosphorylation of tyrosine hydroxylase, the rate-limiting enzyme (Wolf & Roth 1990). Together, these modulatory effects of D2R activation are critical in maintaining the physiological motor control and reward-associated learning functions of DA systems. The importance of autoregulation has been highlighted by a

selective knock-out of D2 autoreceptors in transgenic mice that exhibit hyperactivity and increased sensitivity to cocaine (Bello et al 2011).

1.5 DA Autoregulation in the Str

At the other end of the DA neurons, D2 autoreceptors are also present on the axon terminals in the Str (Sesack et al 1994). Their efficiency and mechanism of autoinhibition, however, is markedly different from their influence in the SNc (Cragg & Greenfield 1997). DA released onto axon terminal autoreceptors in the Str provokes an inhibitory effect on subsequent DA release that is two to three-fold greater than that which occurs in the SNc. This difference in inhibitory strength may be due to the greater density of D2 autoreceptors in the Str, which might resist DA saturation or provide D2Rs that are more spatially accessible than in the SNc (Cragg & Greenfield 1997). Despite the overall increased inhibitory strength of D2 autoreceptors in the Str, these receptors do not affect firing rate as they do in the SNc. They are, however, linked to reduction of DA synthesis similar to the mechanism of autoreceptors the SNc (Farnebo & Hamberger 1971, Kehr et al 1972, Wolf & Roth 1990).

1.6 D2R as Post-Synaptic Receptors and Heteroreceptors

In addition to autoreceptor functions, D2Rs are found on dendrites, spines, soma, and glia in the Str. D2Rs are often observed on MSN spines both adjacent to and far from DA synapses (Hersch et al 1995, Sesack et al 1994, Yung et al 1995). The mixture of perisynaptic and

extrasynaptic D2Rs have been suggested to encode both tonic and phasic DA released onto the MSN (Marcott et al 2014). Unlike autoreceptors, the function of D2 post-synaptic receptors is not to regulate DA release, but instead to regulate the MSN's response to extrinsic glutamatergic and GABAergic input (Smith & Bolam 1990, Yung & Bolam 2000).

In the Str, D2R immunoreactivity is present on axons terminals thought to belong to glutamatergic neurons originating in the cortex and thalamus (Sesack 2010, Sesack et al 1994, Wang & Pickel 2002). D2 heteroreceptor activation results in an inhibition of glutamate release that is selective for terminals with low release probability, so that DA's inhibitory effect bypasses the most active synaptic connections (Bamford et al 2004, Sesack 2010).

1.7 DA release

D2-type postsynaptic receptors and heteroreceptors are reached by DA following classical axonal release in the Str. Action-potential evoked Str DA release is TTX-sensitive, highly dependent on extracellular Ca2+, and released from small clear synaptic vesicles. Given that only about one-third of DA varicosities form identifiable synapses (Descarries et al 1996), it is likely that DA is released from both synaptic and non-synaptic sites (Liu et al 2018).

Compared to axon terminals in the Str, the mechanisms governing somatodendritic DA release in the SNc are not fully understood. Evoked somatodendritic release is certainly TTX-sensitive, implying that release is mediated through a depolarization of membrane potential (Beckstead et al 2004). It also requires extracellular calcium, but at millimolar concentrations much lower than required for axonal release (0.25 mM- 1.5 mM) (Beckstead et al 2004, Chen et al 2011, Rice & Patel 2015). The specific voltage-gated calcium channels that are responsible for

action-potential dependent calcium influx in dendrites have yet to be confirmed, but there is evidence that midbrain somatodendritic DA release requires N- and P/Q-type, but not L-type, calcium channels (Rice & Patel 2015).

The majority of DA dendrites lack the clusters of synaptic vesicles found near axonal or dendrodendritic synapses (see below). Nevertheless, physiological evidence has shown that DA release is most likely quantal and exocytotic (Beckstead et al 2004, Gantz et al 2013, Jaffe et al 1998). A competing theory has also been proposed that DA release can be mediated by reversal of the DA transporter (DAT), although reversal is improbable under normal physiological conditions (Rice & Patel 2015). Instead of small clear synaptic vesicles, dendritic DA appears to be stored in tubulovesicles that are probably extensions of the ser and express the vesicular monoamine transporter-2 (VMAT2) (Nirenberg et al 1996). Dendritic DA release from these tubulovesicles is known to be sensitive to the effects of reserpine, an irreversible VMAT2 blocker (Beckstead et al 2004).

1.8 How is DA Delivered to the Autoreceptor?

The actual route by which DA is transmitted from its point of release to D2Rs in the SNc is contested. Conventional dendrodendritic synapses in the SNc are found only rarely (Groves & Linder 1983), although somatosomatic and dendrodendritic appositions are commonly observed in the nearby VTA (Bayer & Pickel 1990, Groves & Linder 1983). Some electrophysiological studies analyzing the time course of evoked D2-IPSCs suggest a model of spatially tight DA release and receptor activation. When dendritic DA release is evoked, the length of time that DA is present extracellularly is short relative to the time constant of resulting IPSCs on neighboring

neurons. This suggests that the kinetics of the D2R-dependent GIRK channel is the rate determining step for dendrodendritic DA transmission, therefore limiting the possible distance between released DA and its receptor (Ford et al 2009). This supposition is supported by studies showing that the time course of DA transmission elicited by electrically-evoked DA release is faster than that induced by DA iontophoresis (Beckstead et al 2004). The concentration of DA required to elicit a D2R-dependent IPSC is around 100 μM, which further suggests a close localization of DA release and D2R activation, as DA diffuses rapidly in the extracellular space (Courtney & Ford 2014, Cragg & Rice 2004, Ford et al 2009).

With this electrophysiological foundation, our collaborator John Williams at Oregon Health & Science University has proposed a model of non-conventional dendrodendritic "synapses" that lack typical morphological structures but still involve focused DA transmission as evidenced by concentrated D2 receptor expression. This study set out to examine possible anatomical evidence for this model. Together with our colleague, we hypothesized that there would be a large amount of membrane-bound D2R on dendrites directly apposing neighboring dendrites. We also hypothesized that there would be an increased concentration of membrane-bound D2R located at these non-conventional "synapse" sites, forming what our collaborator has referred to as "hot spots" of somatodendritic DA reception.

Previous anatomical studies into the localization of D2R in the ventral midbrain have utilized immunoperoxidase to label these receptors under electron microscopy (Pickel et al 2002, Sesack et al 1994, Yung et al 1995). The benefit of this method is that immunoperoxidase uses signal amplification and is therefore sensitive to lower-concentration proteins like the D2R. The disadvantage of this approach is that peroxidase reaction product is easily diffusible and therefore, at best, reveals the relative subcellular location of D2R (Sesack et al 2006). A more exact

localization of D2R can be obtained by using an anchored silver-enhanced immunogold complex. This method has been used in a wildtype mouse model to analyze D2R in the VTA (Garzon et al 2013). To date, there has not been an analysis of the specific subcellular localization of D2R in the SNc of a mouse utilizing electron microscopy. The previous analysis of the VTA utilizing immunogold suggested that D2Rs are more dispersed, rather than clustered, along the membrane of DA cells. This lack of "hot spot" detectability might be due to immunogold's decreased sensitivity to lower-concentration proteins like D2Rs. This problem could be exacerbated if D2Rs are more spatially inaccessible such as on the inside of a close dendrodendritic apposition.

To combat the decreased sensitivity that accompanies the increased spatial resolution of immunogold labeling, our collaborators at Oregon Health & Science University have developed a transgenic mouse model with an exogenous enhanced green florescent protein (eGFP) tag on the D2R. At Oregon, these eGFP-D2 receptors have been analyzed in the SNc with fluorescence imaging and shown to have a punctate distribution, possibly indicating relatively dense groupings of D2Rs (Robinson et al 2017). Our analysis, utilizing electron microscopic examination of immunogold-labeled eGFP-D2R, should be able to corroborate these findings at a more exact spatial level and provide a comprehensive subcellular localization study of D2R in the SNc.

In the course of our quantitative analysis of the SNc, we determined that a comparative examination of the dorsolateral Str in the same animals would be an important addition to the study. Furthermore, in the SNc, we unexpectedly discovered what appeared to be axon initial segments (AIS) expressing eGFP-D2R. To confirm that these structures were indeed AISs, we performed additional immunolabeling for ankyrin-G and beta IV-spectrin (Huang & Rasband 2018, Leterrier & Dargent 2014) along with the eGFP-D2R.

2.0 Methods

2.1 Subjects

All animal procedures and protocols were conducted in accordance with the National Institute of Health *Guidelines for the Care and Use of Laboratory Animals*.

Perfused transgenic mouse brains, based on the C57BL/6 background strain, were acquired from the laboratory of John Williams, Ph.D., at Oregon Health & Science University. Transcardial perfusions with electron microscopy-grade fixatives were performed by Sue Aicher, Ph.D. at the same institution. The transgenic mouse line had a knock-in of enhanced green fluorescent protein (eGFP) on the amino-terminus of D2Rs and was generated in the Transgenic Mouse Facility at the University of California at Irvine. The procedure for transgenic mouse generation and evidence supporting the normal functionality of eGFP-tagged D2Rs has been published previously (Robinson et al 2017). For the analysis of eGFP-immunogold in the SNc and Str, two separate cohorts of four animals each were perfused at Oregon Health & Science University, and then their brains were shipped to the University of Pittsburgh for examination.

To obtain brain samples, eGFP-D2R transgenic mice were anesthetized with 100 mg/kg sodium pentobarbital i.p. to minimize suffering. They were then injected with 1 g/kg sodium diethyldithiocarbamate, a zinc chelator, so that eventual silver enhancement of pre-embedding immunogold did not bind to endogenous zinc (Veznedaroglu & Milner 1992). After 15 minutes, mice were laid out on a wire mesh rack over a collection tub, and the abdomen was opened so that the heart was accessible. The right atrium was cut to open the cardiovascular system, and a cannula was inserted through the left ventricle into the aorta and clamped into place. The mice were first

perfused with 5-10 ml of saline containing 1000 units/ml of heparin, an anticoagulant. The cardiovascular system was then flushed with a 0.1 M phosphate buffer (pH 7.4) containing one of two fixatives: 12.5 ml of 3.75% acrolein with 2% paraformaldehyde, followed by 50-75 ml of 2% paraformaldehyde, or 50-75 ml of 0.2% glutaraldehyde with 4% paraformaldehyde. This process fixed brain proteins so that tissue could be sectioned and later analyzed in the electron microscope. Following perfusion, brains were extracted from the skull and post-fixed with the last fixative for 30-60 minutes. The brains from Oregon Health & Science University were then stored in phosphate buffer for overnight shipment to our laboratory.

Experimental tests that determined the ideal conditions for localizing antibodies directed against ankyrin-G and beta IV-spectrin were conducted in 12 wildtype mice of strain C57BL/6 at the University of Pittsburgh. Animal perfusion here followed an equivalent procedure to that described above. Afterwards, a third cohort of three eGFP-D2R transgenic mice was perfused, and their brains were sent from the Oregon Health & Science University expressly for dual-labeling of eGFP-D2R and beta IV-spectrin.

2.2 Immunocytochemistry

Fixed brains were cut into blocks containing the midbrain or Str (Figure 1) that were then sectioned at 50 μm on a vibratome. Slices were treated with phosphate buffer containing 1% sodium borohydride to remove excess reactive aldehydes followed by rinsing with phosphate buffer. Slices were transferred to 0.1 M tris-buffered saline (pH 7.6) that contained 3% normal goat serum and 1% bovine serum albumin to block endogenous proteins that might erroneously be labeled by primary or secondary antibodies. The blocking solution also contained

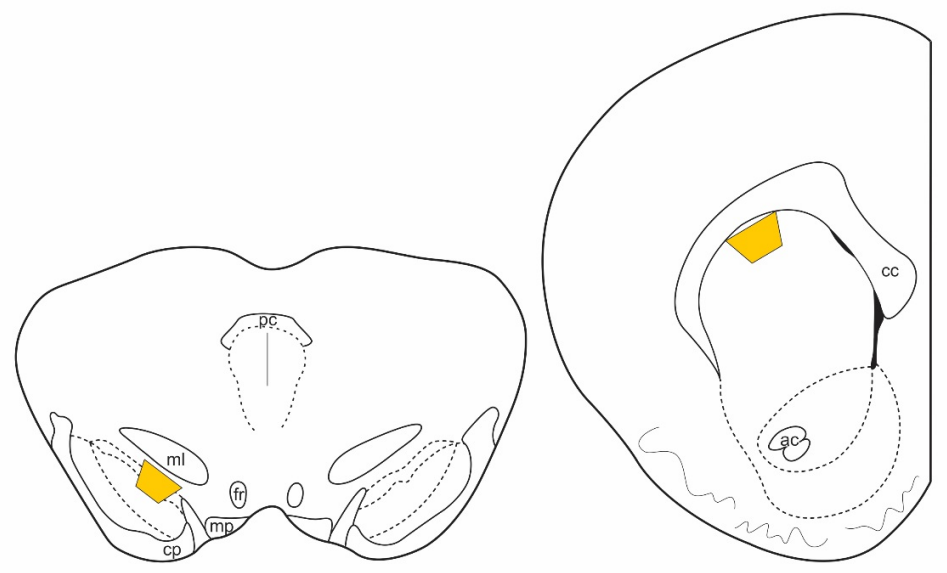

Figure 1: Schematic drawing of the approximate locations of sampling from the SNc and Str in mouse brains

(**Left**) Samples of the SNc (yellow trapezoid) were taken between Bregma coordinates -3.40 mm and -3.64 mm. (**Right**) Samples of the dorsolateral Str (yellow trapezoid) were taken between Bregma coordinates +1.10 mm and -0.10 mm. Landmarks used to locate the target areas included the medial lemniscus (ml), cerebral peduncle (cp), and corpus callosum (cc). Other abbreviations: fasciculus retroflexus (fr), mammillary peduncle (mp), posterior commissure (pc), and anterior commissure (ac).

the detergent Triton-X100 at 0.04% to enhance antibody penetration into cells and processes. Tissue was exposed to this blocking solution for 30 minutes.

For immunogold labeling of the eGFP-D2R, slices were transferred to blocking solution containing eGFP primary antibody at a concentration of either 1:500 or 1:1000. The primary antibody from Avēs Labs, Inc (GFP-1010) was made in chicken against green fluorescent protein. The company brochure indicates that specificity has been tested using Western blot and immunohistochemistry from transgenic mice expressing GFP. In addition, preliminary studies in our laboratory determined that immunostaining of brain sections from non-eGFP expressing animals produced no detectable signal. Slices were incubated in the eGFP primary antibody

overnight at room temperature for 12-15 hours, then rinsed with 0.1 M tris-buffered saline followed by 0.01 M phosphate-buffered saline (pH 7.4).

Tissue was prepared for exposure to the immunogold secondary antibody by being rinsed with a washing buffer containing 3% normal goat serum, 0.8% bovine serum albumin, and 0.1% cold fish gelatin (Aurion). We utilized a secondary antibody that was 0.8 nM gold-conjugated and was made in goat against chicken (Aurion) (Figure 2). Tissue was exposed to the antibody at a 1:50 concentration made in washing buffer and incubated overnight for 12-15 hours at room temperature. Excess immunogold secondary antibody was rinsed off the tissue three times with the washing buffer and three times with phosphate buffered saline. Additional protein fixing was then achieved with exposure to 2.5% glutaraldehyde in phosphate buffered saline for 10 minutes, followed by several rinses in phosphate buffered saline. These antibody-labeled slices were then treated four times for 10 minutes each with Enhancement Conditioning Solution (Aurion) diluted 1:10 with ultrapure water.

To increase the ease of identification of eGFP-D2R immunogold particles under the electron microscope, sections were exposed to an RGENT-SEM proprietary silver enhancement solution (Aurion) for 120-180 minutes. Antibody-complex attachment was stabilized by additional treatments in Enhancement Conditioning Solution for four separate rounds of 10 minutes each, and sections were finally rinsed in 0.1 M phosphate buffer.

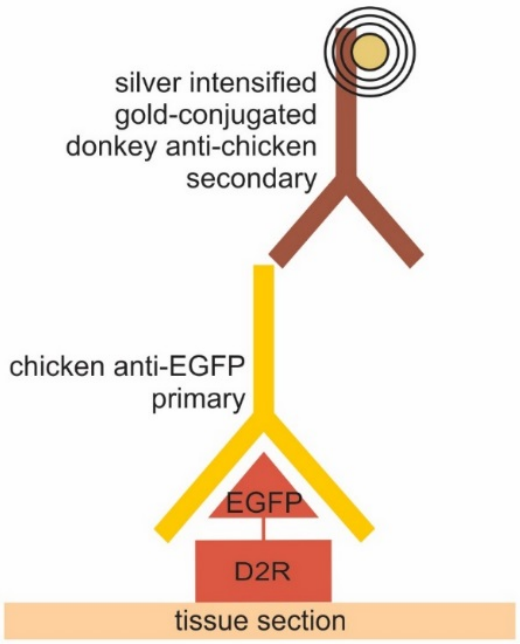

Figure 2: Diagram of the antibody complex utilized to label D2R in eGFP-D2R transgenic mouse brains for analysis with electron microscopy

An exogenous eGFP-tag was attached to the amino-terminus of the D2R in transgenic mice, and an anti-eGFP antibody was directed to sites of eGFP expression. The primary antibody was then localized by an anti-species secondary antibody complex incorporating a gold particle that was subsequently size-enhanced by silver.

In order to test antibodies against ankyrin-G and beta IV-spectrin, wildtype mouse brains were prepared for immunoperoxidase labeling using methods comparable to those used for eGFP labeling. The primary antibody against beta IV-spectrin was an affinity purified polyclonal made in rabbit (gift of Dr. Matthew Rasband, Baylor College of Medicine). The primary antibody against ankyrin-G was made in mouse and purchased from the UC Davis/NIH NeuroMab Facility. The higher quality anti-ankyrin-G antibody used by Henny et al. for DA cell AIS (Gonzalez-Cabrera et al 2017) is no longer available (https://www.buzzfeednews.com/article/danvergano/santa-cruz-biotech-fined-35-million). After 30 minutes in blocking solution, primary antibodies for either ankyrin-G or beta IV-spectrin were added to the blocking solution at concentrations from 1:50 to

1:1000. Slices were incubated overnight for 12-15 hours and washed three times in tris-buffered saline for 10 minutes each. Tissue was then again incubated in appropriate blocking solution to which biotinylated secondary antibodies were added. The secondary antibody for ankyrin-G was anti-mouse made in goat, and the secondary antibody for beta IV-spectrin was anti-rabbit made in goat. Both antibodies were from Vector Laboratories. Tissue was incubated with secondary antibodies at 1:400 for 30 minutes and rinsed another three times in tris-buffered saline for 10 minutes each.

To make the secondary antibodies visible in the electron microscope, antibody-bound tissue was exposed to a 30-minute incubation in an ABC Kit solution containing avidin-biotin peroxidase complex (Vector Laboratories). Slices were again rinsed in tris-buffered saline, three times for five minutes each. Tissue was then exposed for 3.5 minutes to a solution containing diaminobenzidine and hydrogen peroxide, which created a reaction product appearing dark and flocculent under the electron microscope. A final three step rinse in phosphate buffer for 5 minutes each completed immunocytochemical processing.

In order to stain brain tissue for both eGFP-D2R and a marker for the AIS, eGFP-D2R transgenic mouse brains were prepared for immunolabeling similar to the previously mentioned procedures. A mixture of primary antibodies, eGFP-D2R at 1:1000, and beta IV-spectrin at 1:100, produced the best signal for dual-labeling in acrolein-fixed brain sections. The procedures for antibody exposure of these two antibody complexes follow those described above, except that primary antibodies for both eGFP and beta IV-spectrin were added at the same time. Immunoperoxidase processing occurred before immunogold processing, and silver enhancement was carried out for only 60-70 minutes.

2.3 Electron Microscope Tissue Preparation

After tissue fixation and antibody exposure, lipids in brain slices were fixed with a bath of 1% osmium tetroxide in 0.1 M phosphate buffer for one hour. After rinsing in phosphate buffer, the tissue was prepared for transmission electron microscope analysis by serial dehydration. Tissue was exposed in five-minute increments to increasing concentrations of ethanol in water: 30%, 50%, 70%, 95%, and two rounds of 100% ethanol. This was followed by two five-minute rounds in propylene oxide.

To further stabilize the tissue for electron microscopy, samples were placed overnight in 1:1 propylene oxide and epoxy resin (EM-Bed 812, Electron Microscopy Sciences). Slices were then transferred to 100% epoxy resin for 2-3 hours before being flat-embedded between two clear commercial plastic sheets. The resin was cured at 60°C for 72 hours until solid. Sections of this flat-embedded tissue were cut to include the areas of interest, either SNc or Str. These cut sections were glued and then baked onto blocks of solid epoxy resin, which allowed for easier trimming of the tissue. The section was trimmed into a trapezoidal shape that included the area of interest, identified with landmarks such as blood vessels and major white matter tracts (Figure 1).

After trimming, ultrathin sections (60 nm) were sliced off the resin block using an ultramicrotome and collected onto 400 mesh copper grids.

As a final preparation for electron microscope analysis, the grid-bound tissue was counterstained with the heavy metals uranyl acetate and lead citrate. This enhanced the visual contrast of lipid membranes when viewed in the transmission electron microscope.

2.4 Electron Microscope Examination

Antibody-stained, grid-bound tissue was observed using an FEI Morgagni transmission electron microscope. Only one ultrathin section from a grid was selected for initial analysis, so as to not double-count immunopositive profiles in near z-plane sections. The trapezoidal areas were redrawn in a gridded lab notebook to map out and record the location of captured micrographs. Squares chosen for analysis ideally consisted of a relatively equal interface between tissue and resin, as this depth maximized both cell morphology and antibody penetration. Squares immediately adjacent to this interface zone were also examined. Chosen grid squares were surveyed in their entirety at 18000X magnification. Regions were captured when the field of the micrograph contained at least one seemingly immunopositive neuronal profile, centered in the micrograph as best as possible. Approximately 15 micrographs were captured from each section of tissue, with most micrographs containing many more than one labeled profile. At least two sections per animal were examined.

2.5 Immunopositive Profile Analysis

The MicroBrightField Neurolucida program v.9 was used to analyze immunopositive neuronal profiles. A profile labeled with immunogold was considered immunopositive for eGFP-D2R if it contained at least three gold particles, regardless of particle location (i.e. plasma membrane or intracellular). Neurolucida was used to trace and quantify the perimeter and area of labeled profile cross-sections, while profile short-axis diameter was manually measured on the micrographs using a ruler.

In order to compare prevalence and density of eGFP-D2R in different profiles and their compartments, immunopositive structures were identified based on established morphological characteristics (Peters et al 1991). Axon terminals were identified by their round structure and concentrations of small clear vesicles typically clustered near a synapse. If axon terminals visibly formed a synapse, the type of synapse was recorded. Asymmetric synapses had thick post-synaptic densities, whereas symmetric synapses did not. Dendrites were recognized by their larger size, smoothly contoured membranes, organelle content (including mitochondria, ser, and Golgi apparatus), and receipt of synapses. Spines were identified primarily by their smaller size, absence of mitochondria, and tendency to be located post-synaptic to an axon terminal forming an asymmetric synapse. Spiny dendrites, like those found in the Str, were differentiated by having necks of spines visibly branching off a dendritic shaft. Astrocytes were identified by their vacuous cytoplasm and serpentine shape, often becoming markedly narrow to fill in spaces between other cellular profiles. Structures were considered unidentified if they lacked substantially distinguishing traits in single section, which tended to happen more in cases of smaller profiles.

The location of immunogold particles within neuronal profiles was also determined using Neurolucida. The eGFP-D2R were considered to be associated with an organelle or the plasma membrane if the corresponding immunogold particle was within 20 nm of the visible structure, as determined using a 20 nm cursor in Neurolucida. This distance was chosen based on the approximate size of antibodies and the corresponding length of the immunogold antibody complex (Mathiisen et al 2006). In the analysis of membrane-bound eGFP-D2Rs, the neighboring cellular profile immediately apposing each gold particle was also identified and recorded: dendrite, axon, glia, or unidentified.

For each type of immunoreactive profile in each animal, the amount of membrane-bound immunogold was totaled and compared to the profile's perimeter to determine an average density of immunolabeling per perimeter. Similarly, the amount of total immunogold was summed and compared to the profile's area to determine an average density of immunolabeling per area. Statistical comparisons that involved proportions of membrane-bound immunogold or overall density of immunolabeling utilized Student t-tests that assumed equal variance. All p values reported here were two-tailed. Categorical comparison of synapse type formed by immunolabeled axons between SNc and Str were determined with Fisher's Exact Test, which is the most sensitive test for two-by-two comparisons.

3.0 Results

3.1 D2R in the SNc

Although tissue was acquired from two separate cohorts of four mice each, no discernable differences were found between the cohorts in terms of location or prevalence of eGFP-D2R immunolabeling. Therefore, the cohorts were analyzed together. Directing antibodies to an eGFP tag on the D2R appeared qualitatively to increase overall immunoreactivity for the receptor compared to prior observations of direct immunogold labeling for D2R in the midbrain (Garzon et al 2013). eGFP-D2R associated immunogold was observed in soma, dendrites, axons, and astrocytes in the SNc, although our quantitative analysis focused only on dendrites and axon terminals. For this analysis, dendrites comprised the majority (66%) of immunogold-labeled eGFP-D2R profiles counted in the SNc, the rest being axon terminals (34%).

3.1.1 D2R in SNc Dendrites

A total of 379 eGFP-D2R immunopositive dendrites were analyzed. The majority of immunogold labeling of dendrites was located intracellularly (72%) (Table 1), as opposed to being on the plasma membrane (28%) (Table 2). Of the intracellular immunogold particles, 79% were observed to be unassociated with neuronal organelles, 17% were visibly associated with the ser, and 4% were located in multivesicular bodies (MV bodies) (Fig. 3). In soma and the most proximal dendrites near the soma (not analyzed quantitatively), gold for eGFP-D2R was also observed around the rough ER and Golgi bodies (Fig. 3). Some immunogold was found in close proximity

Table 1: Distribution of Intracellular eGFP-D2R Gold Particles within Dendrites of the Mouse SNc

Mouse	eGFP-D2R Labeled Dendrites	Average Dendrite Area (μm^2)	Total Gold Particles per Dendrite Area ($\#/\mu m^2$)	Number (%) Intracellular Gold Particles	Organelle Associated w/ Intracellular Gold Particles		
					Smooth ER	MV body	None
1	100	2.37	5.30	724 77%	48 7%	42 6%	634 88%
2	44	3.02	5.46	351 66%	52 15%	22 6%	277 79%
3	51	2.48	3.50	252 76%	25 10%	5 2%	222 87%
4	33	2.96	5.06	231 73%	39 17%	17 7%	175 76%
5	34	3.19	4.16	208 82%	50 24%	4 2%	154 75%
6	30	1.31	10.80	190 64%	41 22%	9 5%	140 74%
7	64	2.11	6.53	354 68%	73 21%	6 2%	275 75%
8	23	2.72	7.70	117 69%	27 23%	1 1%	89 76%
N **mean** **sem**	379	2.52 0.22	6.06 0.82	**72%**	17%	4%	79%

Table 2: Distribution of Memebrane-Bound eGFP-D2R Gold Particles on Dendrites of the Mouse SNc

Mouse	eGFP-D2R Labeled Dendrites	Average Dendrite Perimeter (µm)	Number (%) Gold Particles on Membrane	Membrane Gold Particles per Dendrite Perimeter (#/µm)	Structure Apposed to Membrane Gold Particles			
					Axon Terminal	Astrocyte	Dendrite	Unidentifiable
1	100	6.93	211 23%	0.33	67 32%	34 16%	42 20%	68 32%
2	44	8.56	177 34%	0.53	91 51%	13 7%	15 8%	58 33%
3	51	6.96	78 24%	0.27	40 51%	21 27%	6 8%	11 14%
4	33	7.89	84 27%	0.44	31 36%	15 18%	5 6%	33 39%
5	34	7.75	47 18%	0.24	30 64%	10 21%	0 0%	7 15%
6	30	5.21	109 36%	0.76	23 21%	32 29%	4 4%	50 46%
7	64	6.41	170 32%	0.50	56 32%	48 28%	3 2%	63 37%
8	23	6.28	53 31%	0.45	17 32%	2 4%	3 6%	31 58%
N **mean** **sem**	379	7.00 0.37	**28%**	0.44 0.06	40%	19%	**7%**	34%

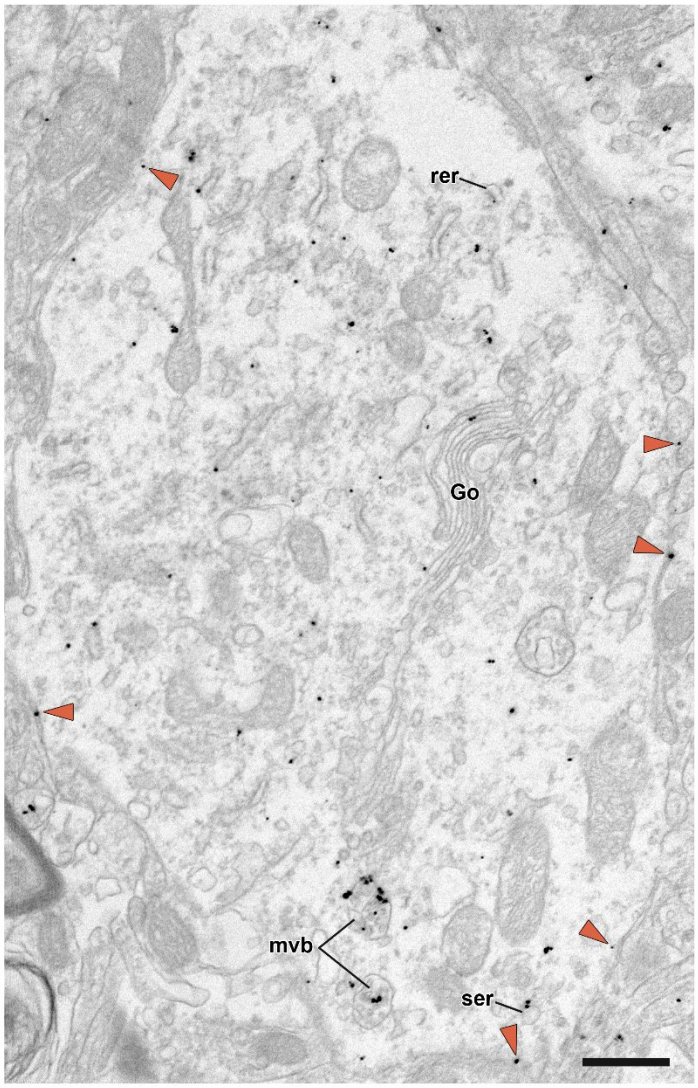

Figure 3: Electron micrograph of an eGFP-D2R immunogold labeled proximal dendrite in the mouse SNc

Immunogold labeling is contained mainly intracellularly and is less frequently spread difusely along the plasma membrane (orange arrowheads). Intracellular immunogold particles are associated with rough endoplasmic reticulum (rer), smooth endoplasmic reticulum (ser), Golgi apparatus (Go), and multivesicular bodies (mvb). Scale bar 0.6 µm.

to mitochondria, but as D2Rs have no known functional relationship with mitochondria, these immunogold particles were classed as having no association. It should be noted that the large amount of immunogold particles having no apparent organelle association may be explained by the nature of single section analysis, such that associated organelles were likely out of the plane of section.

The prevalence of eGFP-D2R bound to dendritic membranes appeared to vary with dendritic diameter (Figs. 3-5). eGFP-D2R immunogold was more likely to be found intracellularly in proximal dendrites (Fig. 3), while the proportion of gold particles representing receptors bound to the membrane was higher in distal dendrites (Figs. 4-5).

The vast majority of dendritic membrane-bound eGFP-D2R was observed to be dispersed along the membrane (Fig. 4). Rarely, three or more immunogold particles appeared to be grouped together at one portion of the membrane (Fig. 6). Such sites were always examined in serial sections where the groupings typically did not continue far in the z-axis (Fig. 6 insert). This observation suggests that sites of potentially high D2R density were spatially restricted in the 60-120 nanometer range.

eGFP-D2R labeled dendrites were observed to receive both symmetric (Figure 4A, C) and asymmetric (Figure 4C) synapses from both immunopositive and immunonegative axon terminals. Rarely, traditional dendrodendritic synapses were observed between two eGFP-D2R labeled dendrites (Figure 7). Immunogold labeling could sometimes be dense at these sites.

In order to determine the presence of possible D2R-mediated dendrodendritic communication sites (distinct from traditional synapses), each membrane-bound gold particle representing eGFP-D2R in the SNc was analyzed for its immediately neighboring cellular profile (Table 2). 40% of membrane-bound immunogold particles were determined to be directly apposed

to axon terminals (Fig. 4A, C), although gold labeling was rarely observed in or near conventional post-synaptic densities (Fig. 4C). Only 7% of dendritic membrane-bound eGFP-D2R immunogold in the SNc was found directly apposed to other dendrites (Fig. 7). A larger amount of immunogold was found directly apposed to astrocytes. The remaining gold particles representing eGFP-D2R occurred across from profiles that could not be identified in single sections. Had a serial section analysis been conducted, it is assumed that these unidentified profiles would sort proportionally into the recognized categories of neighboring structures.

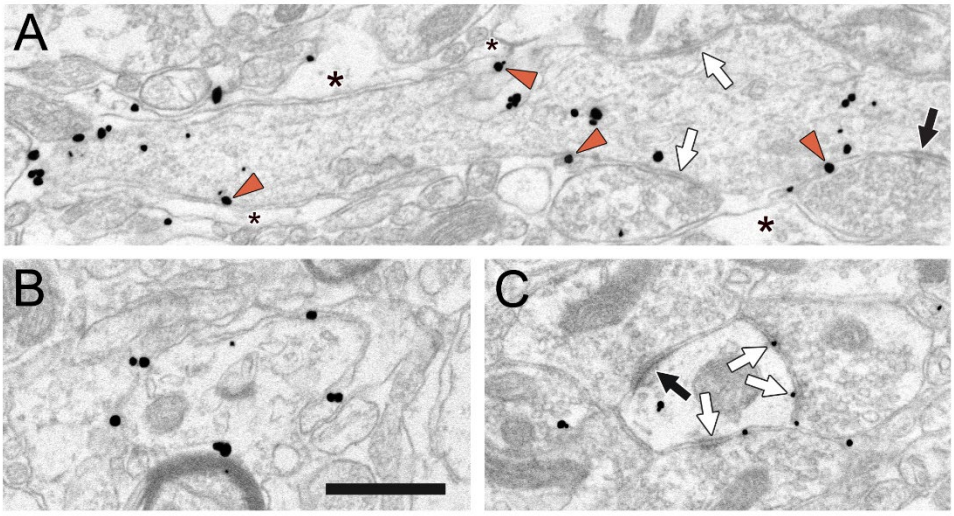

Figure 4: Electron micrographs of eGFP-D2R immunogold labeled distal dendrites in the SNc

(**A**) eGFP-D2R immunogold is commonly bound to the cell membrane (orange arrowheads), where it is randomly dispersed and adjacent to axon terminals and astrocytes (asterisk). The dense membrane accumulation of gold particles at the left of this dendrite was examined in serial sections, but the gold labeling did not recur. The dendrite receives symmetric synapses (white arrows) and asymmetric synapses (black arrow) from non-labeled axon terminals. (**B**) An atypical immunopositive distal dendrite contains only eGFP-D2R bound to the membrane. (**C**) Along with multiple symmetric synapses, this labeled dendrite receives an asymmetric synapse from an axon terminal. Dendritic membrane-bound immunogold particles are rarely found within or near synapses, as shown here to the right. Scale bar, 0.6 µm.

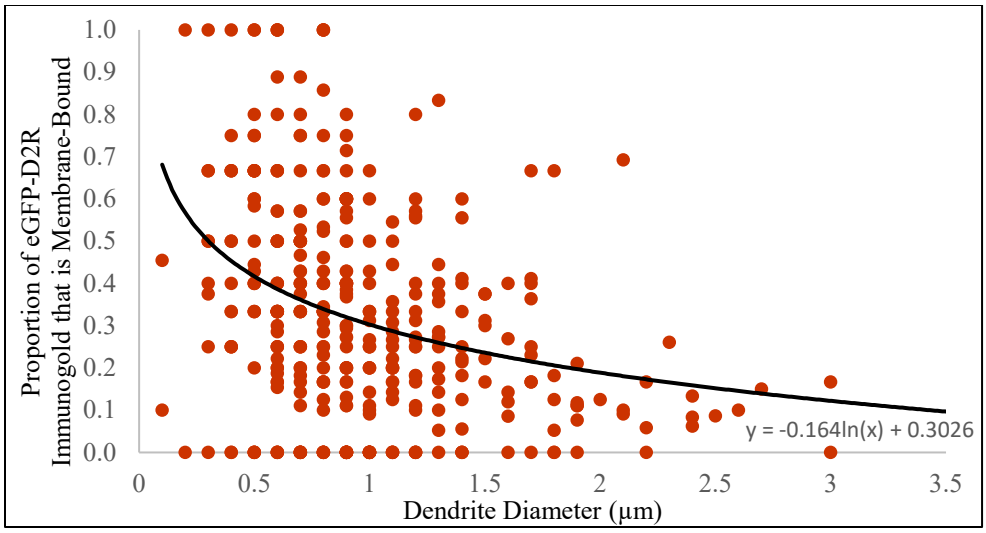

Figure 5: Scatterplot showing that the proportion of eGFP-D2R membrane gold in the mouse SNc varies by dendrite diameter

The short-axis diameter of individual labeled dendritic profiles is plotted against the proportion of immunogold on the membrane. A simple logarithmic line of best fit is also plotted (black curved line).

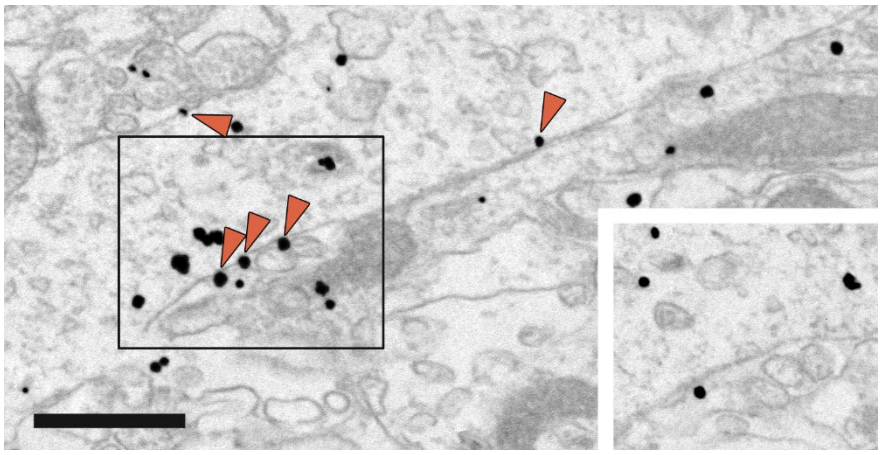

Figure 6: Rare electron micrograph of multiple eGFP-D2R immunogold particles found tightly grouped on an area of the dendritic membrane in the SNc

In addition to gold particles individually associated with the plamsa membrane (orange arrowheads), a grouping of membrane-bound immunogold is found on a distal dendrite (black boxed region. In most cases, when these particle groupings are examined in serial sections of the relevant membrane region, the grouping does not continue far into the z-plane (insert). Scale bar, 0.6 µm.

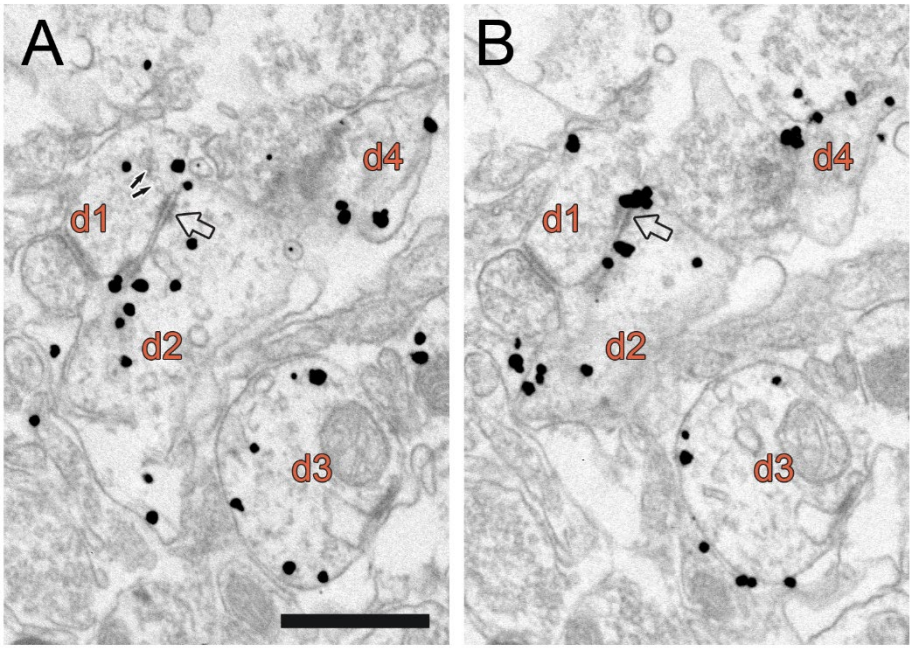

Figure 7: Serial electron micrographs of four eGFP-D2R immunogold labeled dendrites in the SNc

A rare dendrodendritic synapse is visible between dendrite (d) 1 and d2 (transparent arrow). Small arrows in (**A**) indicate accumulated vesicles in close proximity to this site. Membrane-bound eGFP-D2R is also found associated with this synapse, as visible in (**B**). d3 and d4 show preferential membrane-associated eGFP-D2R.

Scale bar, 0.6 µm.

3.1.2 D2R in SNc Axon Terminals

eGFP-D2R immunoreactivity was also found in axon terminals of the SNc (Tables 3, 4). Similar to labeling in nigral dendrites, immunogold particles in axon terminals were observed to be intracellular (76%) more often than on the membrane (24%) (Figure 8). 62% of labeled axon terminals formed no synapses visible in the single sections analyzed. Of those immunopositive axon terminals that did form synapses, more were of the symmetric type (32%) (Fig. 8C) than asymmetric (6%) (Fig. 8D). The profiles immediately across from eGFP-D2R immunogold particles bound to the membrane were analyzed in a manner similar to that for dendrites. In this

case, the majority of gold particles were found to be apposed to dendrites, followed by axon terminals and astrocytes, with the remainder of profiles being unidentified in single sections (Table 4). The fact that most of the gold particles on axonal membranes were found adjacent to dendrites suggests that the relative infrequency of this occurrence for gold particles on the membranes of dendrites (Table 2) was not due to technical issues.

3.1.3 D2R in SNc Axon Initial Segments

During this ultrastructural investigation, eGFP-D2R immunogold was occasionally found in association with profiles in the SNc that did not contain accumulated vesicles but also did not appear to be dendrites. Instead, their morphology showed a dense undercoating under the plasma membrane and an enlarged surrounding extracellular space that sometimes contained granules. These characteristics suggested that they were AISs (Fig. 9). These presumed AIS profiles appeared to contain denser eGFP-D2R immunogold than either labeled dendrites or axon terminals in the SNc (based on total immunogold per area; compare Table 5 with Tables 1 and 3, respectively). This difference was not analyzed statistically, however, because of the small sample of these immunopositive putative AIS profiles in our analysis.

On the presumed AIS structures, in addition to the immunogold particles meeting the 20 nm criterion for membrane association, there tended to be a distinct collection of particles found ~40 nm from the plasma membrane, just beneath the dense undercoating (Fig. 9). We classified these gold particles as being “near” membrane-bound eGFP-D2R (Table 5). Together with the immunogold meeting the criterion of less than 20 nm from the membrane, these particles composed the majority of AIS labeling (70%). The remaining particles were intracellular (30%).

Table 3: Distribution of eGFP-D2R Gold Particles within Axon Terminals of the Mouse SNc

Mouse	Number eGFP-D2R Labeled Axon Terminals	Average Terminal Area (μm^2)	Total Gold Particles per Terminal Area ($\#/\mu m^2$)	Number (%) Intracellular Gold Particles	Synapses Formed by Axon Terminals		
					Symmetric	Asymmetric	None
1	27	0.68	8.31	97 78%	9	1	17
2	5	0.83	7.38	21 81%	0	1	4
3	3	1.02	3.65	8 89%	1	0	2
4	11	1.17	6.31	36 77%	3	0	8
5	26	0.59	11.52	73 68%	11	0	15
6	17	0.69	10.13	65 71%	5	0	12
7	64	0.71	7.59	164 67%	19	3	26
8	38	1.10	4.35	109 76%	8	6	24
N	191				56	11	108
mean		0.85	7.41	**76%**	32%	6%	62%
sem		0.08	0.94				

Table 4: Distribution of Memebrane-Bound eGFP-D2R Gold Particles on Axon Terminals of the Mouse SNc

Mouse	Number eGFP-D2R Labeled Axon Terminals	Average Terminal Perimeter (µm)	Membrane Gold Particles per Terminal Perimeter (#/µm)	Number (%) Gold Particles on Membrane	Structure Apposed to Membrane Gold Particles			
					Dendrite	Axon Terminal	Astrocyte	Unidentifiable
1	27	3.58	0.31	27 22%	6 22%	9 33%	3 11%	9 33%
2	5	4.43	0.18	5 19%	2 40%	2 40%	0 0%	1 20%
3	3	4.47	0.09	1 11%	1 100%	0 0%	0 0%	0 0%
4	11	3.91	0.30	11 23%	3 27%	1 9%	3 27%	4 36%
5	26	2.97	0.55	35 32%	3 9%	16 45%	12 34%	4 11%
6	17	3.57	0.51	27 29%	5 19%	5 19%	4 15%	13 48%
7	64	3.32	0.45	80 33%	15 19%	26 33%	16 20%	23 29%
8	38	4.74	0.21	35 24%	6 17%	8 22%	1 3%	20 57%
N **mean** **sem**	191	3.87 0.22	0.33 0.06	**24%**	32%	25%	14%	29%

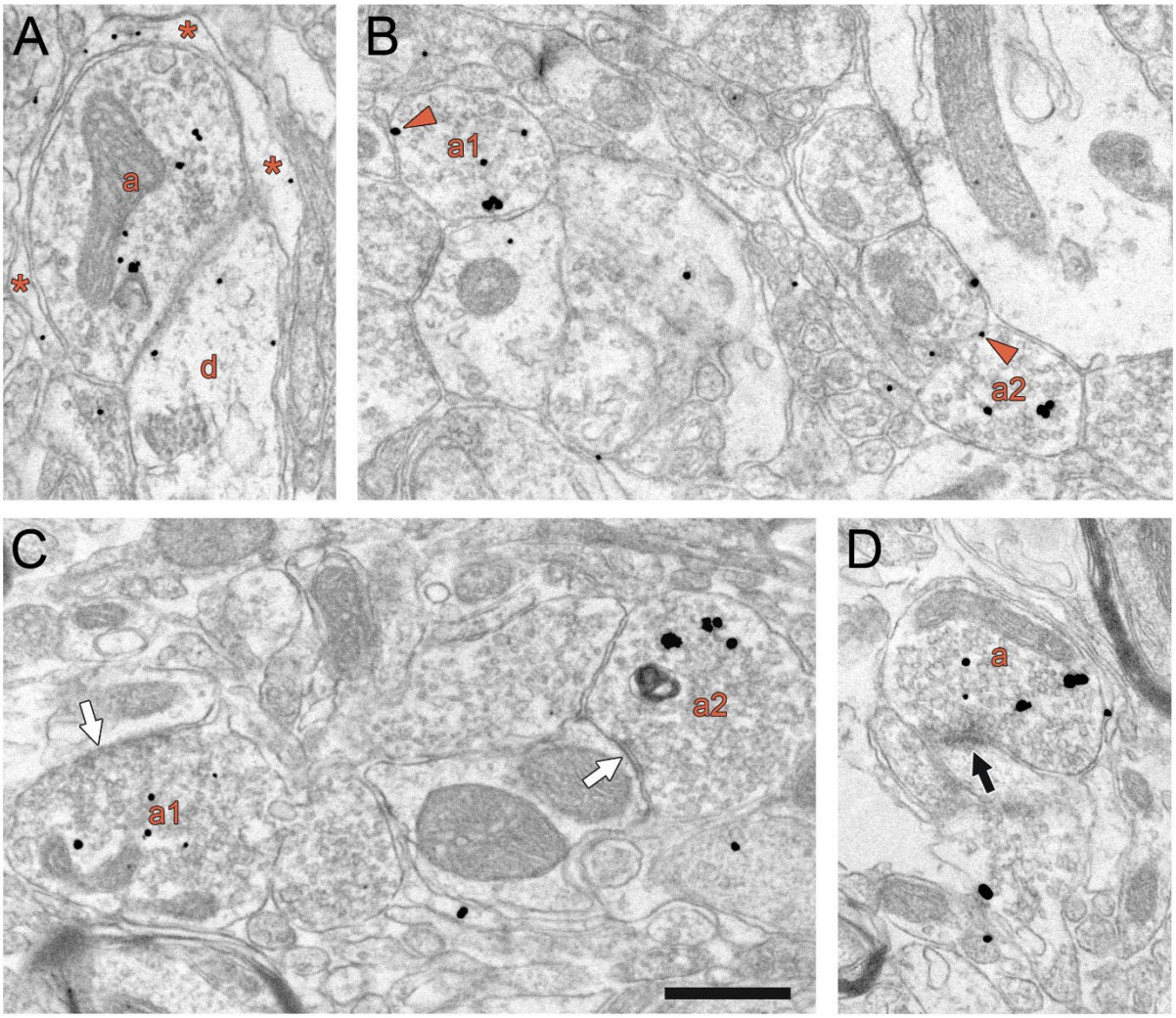

Figure 8: Electron micrographs of eGFP-D2R immunogold-labeled axon terminals in the SNc

(**A**) Immunogold-labeling tends to be located intracellularly in axon terminals. In this case, the axon (a) is surrounded by an immunopositive astrocyte (asterisks) and apposed to an immunopositive dendrite (d). (**B**) eGFP-D2R immunogold is also sometimes observed bound to the plasma membrane (orange arrowheads), in these cases at sites directly apposed to unlabeled axon terminals. (**C-D**) Immunopositive axon terminals sometimes form symmetric (white arrows) or asymmetric synapses (black arrow) with dendrites. Scale bar, 0.6 µm.

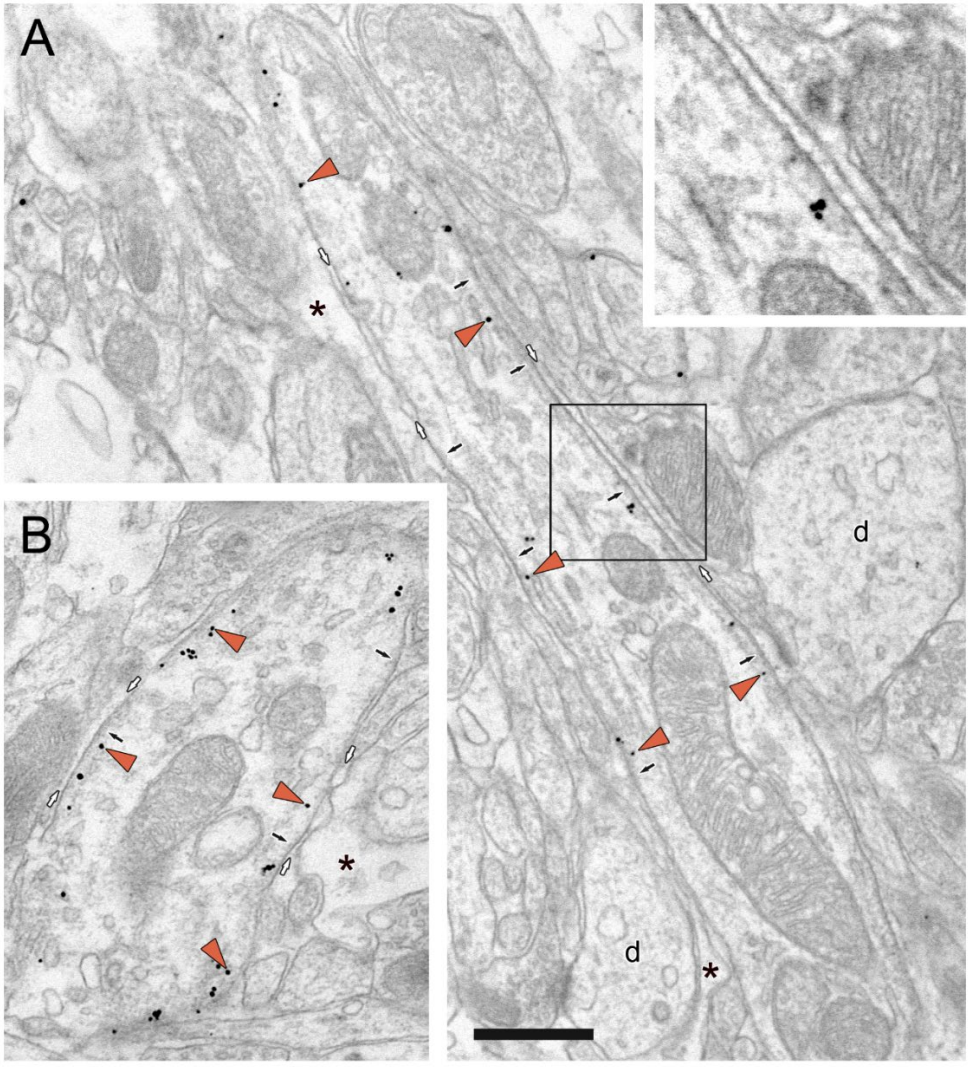

Figure 9: Electron micrographs of presumed axon initial segments in the SNc labeled with eGFP-D2R immunogold

(**A-B**) eGFP-D2R labeled profiles appearing distinct from nearby dendrites (d) exhibit morphological traits characteristic of axon initial segments, including a dense submembrane undercoating (small black arrows) and enlargement of the surrounding extracellular space (small white arrows), that intermittently contains granules (top right insert corresponding to the black boxed region in A). Astrocytes (asterisks) are also found adjacent to these structures. Along with eGFP-D2R immunogold that is bound to the membrane, immunogold particles are also frequently found just under the dense undercoating, at roughly <40 nm from the membrane (orange arrowheads). Presumed AIS profiles were examined in serial sections whenever possible, and none were found to receive synaptic input. Scale bar, 0.6 µm.

Table 5: Distribution of eGFP-D2R Gold Particles within Presumed Axon Initial Segments of the Mouse SNc

Mouse	eGFP-D2R Labeled AIS	Total Gold Particles per AIS Area (#/µm²)	Membrane Gold Particles per AIS Perimeter (#/µm)	Number (%) Gold Particles on Membrane	Number (%) Gold Particles Near (~40 nm) the Membrane	Number (%) Intracellular Gold Particles
1	1	15.55	1.65	12 27%	15 34%	17 39%
3	2	6.20	0.59	9 33%	5 19%	13 48%
		6.99	0.13	1 9%	2 18%	8 73%
4	1	12.49	0.89	3 33%	3 33%	3 33%
5	1	17.17	1.79	7 78%	0 0%	2 22%
6	2	13.74	0.87	4 67%	1 17%	1 17%
		5.98	1.14	3 100%	0 0%	0 0%
7	1	18.80	1.07	5 19%	10 38%	11 42%
8	1	12.92	0.00	0 0%	5 100%	0 0%
N **mean** **stdev**	9	12.20 4.80	0.90 0.58	**41%**	**29%**	**30%**

In an attempt to verify the presence of D2R in the AIS of the SNc, a subsequent study was conducted to dually label profiles with markers for both the AIS and the eGFP-D2R. Immunoperoxidase antibody complexes against either ankyrin-G or beta IV-spectrin, which are both found in AISs as well as nodes of Ranvier, were tested in wildtype mouse SNcs. Antibodies against beta IV-spectrin (but not ankyrin-G) were determined to label well in the fixative that was

also ideal for eGFP-D2R immunogold (Fig. 10). A separate cohort of eGFP-D2R transgenic mice was then processed for dual immunoperoxidase for beta-IV spectrin and immunogold for eGFP-D2R. To date, some degree of colocalization of these markers has been found, confirming the presence of the D2R on the AIS in this region (Figure 11).

3.2 D2R in the Str

The prevalence of eGFP-D2R bound to the membrane of SNc dendrites seemed to be lower than initial predictions made by our lab as well as by our colleague John Williams, based on fluorescence light microscopy. To ensure that our ultrastructural immunocytochemical approach did not unduly limit detection of eGFP-D2R, a comparison was made to the principal target of SNc DA neurons, the dorsolateral Str. In this region, D2R expression by dendrites represents a post-synaptic site known to be in higher concentrations relative to the SNc. The tissue used for striatal analysis originated from the same animals used in the SNc analysis and was processed at the same time with identical procedures and batches of antibody solutions. Again, no noticeable differences in eGFP-D2R immunolabeling in the Str were observed between the two animal cohorts.

As in the SNc, eGFP-D2R labeling in the Str was more frequently observed in dendrites (78%) than axon terminals (22%) (Fig. 12; Table 6). Similarly, both immunopositive soma and astrocytes were also observed in the Str but were not evaluated in this study.

eGFP-D2R immunopositive dendrites in the Str were significantly more densely labeled than dendrites in the SNc (Table 6; $p=0.0006$). Additionally, eGFP-D2R was significantly more

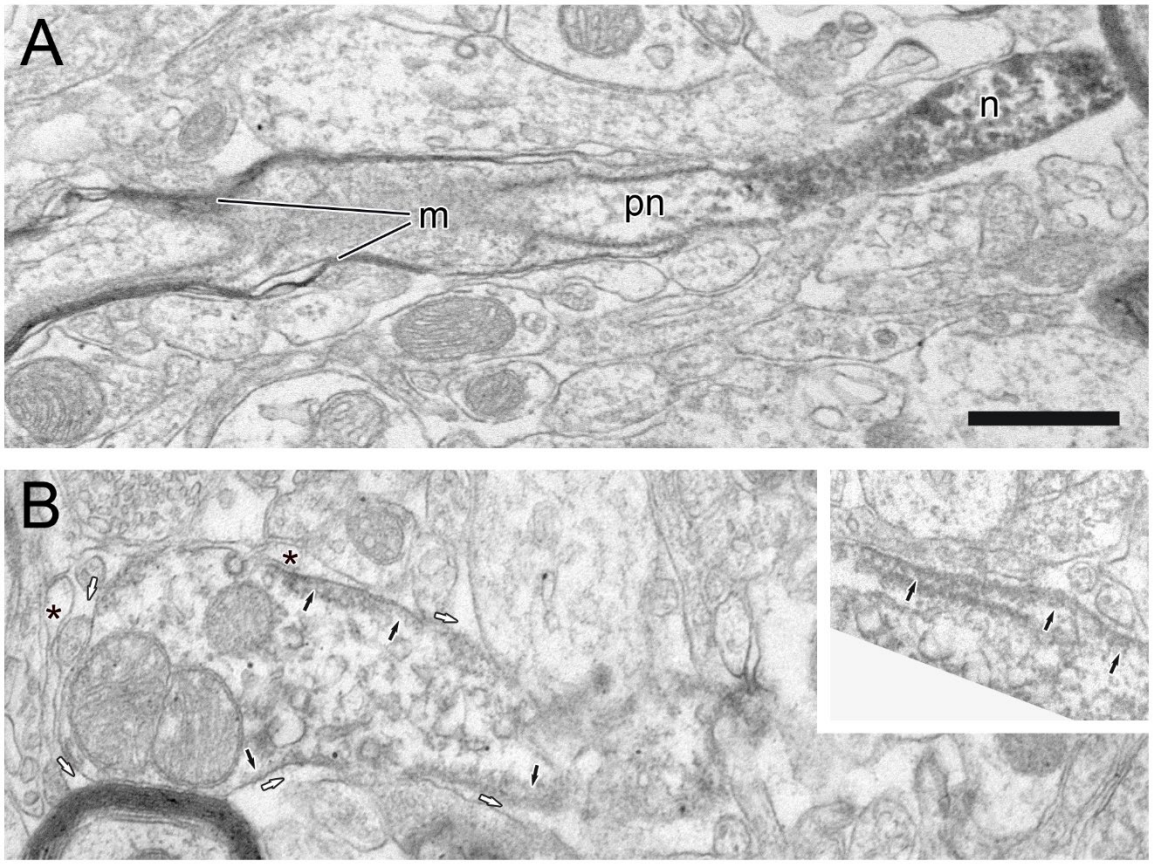

Figure 10: Electron micrographs of SNc profiles single-labeled with immunoperoxidase for beta IV-spectrin

(**A**) Immunoperoxidase for beta IV-spectrin labels a node of Ranvier (n) and paranode region (pn) of a myelinated axon. Diffuse, dark flocculent peroxidase reaction product is most prominent in the region of the node, and decreases through the paranode and further along the axon as visible layers of myelin (m) begin their ensheathment. (**B**) An axon initial segment displays both light immunoperoxidase product for beta IV-spectrin as well as a characteristic dense submembrane undercoating (small black arrows) and enlarged extracellular space (small white arrows). This profile is also apposed by astrocytes (asterisks). AIS profiles were distinguished from nodes of Ranvier by examination in serial sections whenever possible. In a serial section through this AIS (insert), the immunoperoxidase reaction product is most evident in association with the dense submembrane undercoating. Scale bar, 0.6 μm.

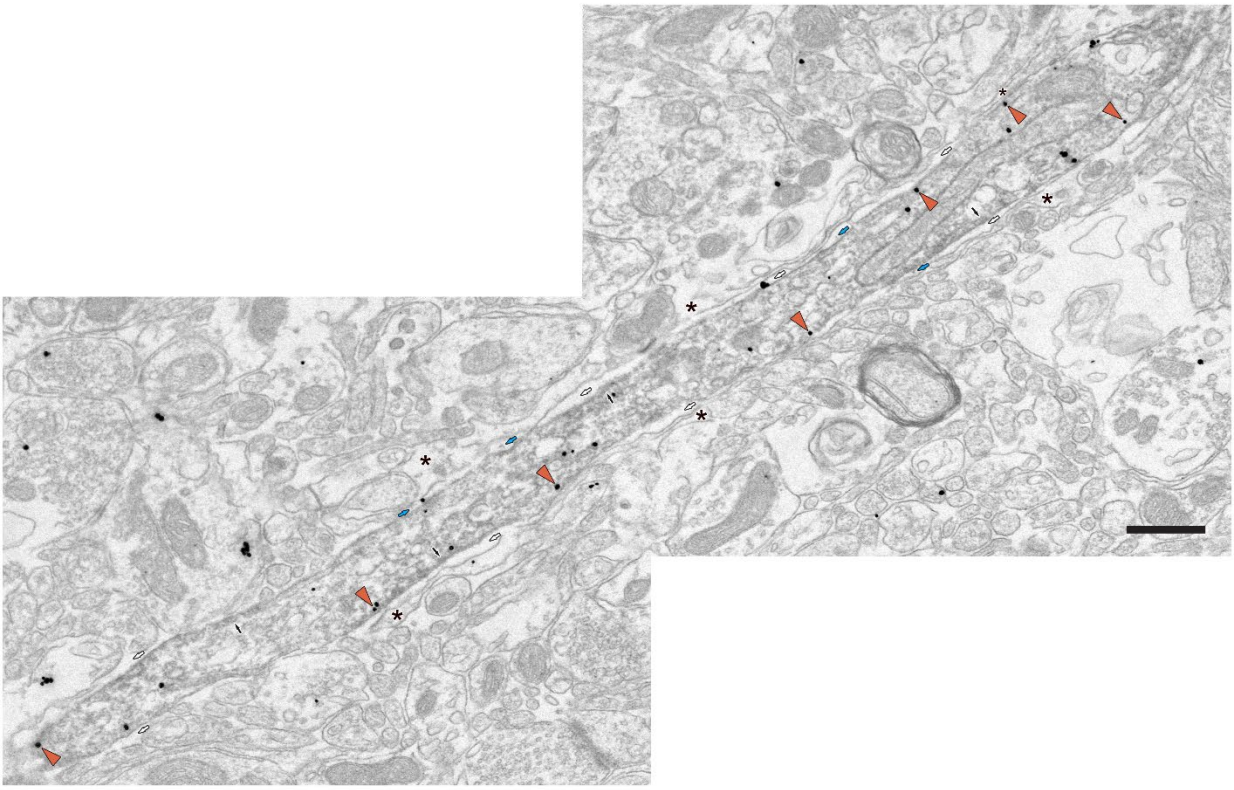

Figure 11: Electron micrograph montage showing an AIS profile dually-labeled with both immunogold for eGFP-D2R and immunoperoxidase for beta IV-spectrin in the mouse SNc

Immunogold particles associated with eGFP-D2R are mainly observed bound to (<20 nm) or near (~40 nm) the plasma membrane (orange arrowheads). Some immunogold is also found intracellularly. Dark, flocculent immunoperoxidase product is visible throughout the AIS and is sometimes particularly heavy just below the plasma membrane in the region of the dense undercoating (small black arrows). Another morphological characteristic that helps to identify this profile as an AIS is the enlarged surrounding extracellular space (small white arrows), which sometimes contains granules (small blue arrows). Astrocytic processes (asterisks) are also visible. Scale bar, 0.6 µm.

likely to be observed bound to the dendritic membrane in the Str than in the SNc ($p=0.000004$) (Fig. 13).

Because striatal neurons have especially spiny dendrites, and these spines are a main target of DA axons terminals, isolated spines were also analyzed independently (Table 7). Dendrites emitting spines in the same plane of the micrograph were still classified as dendrites (Fig. 13). Independently-analyzed spines contained a higher proportion of eGFP-D2R labeling on the membrane (versus intracellular) than dendrites in the Str ($p=0.002$).

eGFP-D2R labeling was also observed in association with axon terminals in the Str (Fig. 13; Table 8). Like dendrites, these axon terminals also were significantly more densely labeled (total immunogold per area) than those in the SNc ($p=0.0064$) and contained immunogold particles that were significantly more often on the membrane ($p=0.000009$).

Most immunopositive Str axon terminals (80%) did not produce visible synapses in the single plane of section analyzed. Those that did, however, were more likely to produce asymmetric synapses as opposed to symmetric. This observation significantly contrasts the prevalence of synapse types formed by eGFP-D2R labeled axon terminals in the SNc (Fisher's Exact Test $p<0.00001$).

Presumed AISs were also found labeled for eGFP-D2R in the Str (data not shown) and demonstrated similar morphological features and subcellular localization of eGFP-D2R as described for the SNc.

Table 6: Distribution of eGFP-D2R Gold Particles within Spiny Dendrites of the Mouse Str

Mouse	Number (%) eGFP-D2R Labeled Profiles	Average Dendrite Area (μm^2)	Total Gold Particles per Dendrite Area ($\#/\mu m^2$)	Average Dendrite Perimeter (μm)	Membrane Gold Particles per Dendrite Perimeter ($\#/\mu m$)	Number (%) Gold Particles on Membrane	Number (%) Intracellular Gold Particles
1	94	1.04	16.33	4.36	0.61	441 61%	278 39%
2	86	0.86	14.58	4.79	0.67	425 67%	207 33%
3	39	1.30	15.71	5.47	0.63	147 63%	87 37%
4	71	0.72	11.62	4.17	0.70	262 70%	111 30%
5	14	1.79	6.98	6.88	0.50	36 50%	36 50%
6	33	0.78	12.25	4.57	0.63	149 63%	86 37%
7	62	1.20	15.52	5.73	0.83	347 83%	71 17%
8	14	1.31	8.40	5.97	0.44	51 44%	65 56%
N **mean** **sem**	413	 1.13 0.12	 12.67 1.24	 5.24 0.33	 0.63 0.04	**63%**	**37%**

Table 7: Distribution of eGFP-D2R Gold Particles between Dendrites and Spines of the Mouse Str

Mouse	Number eGFP-D2R Labeled Profiles	Dendrites				Spines			
		Number eGFP-D2R Labeled Dendrites	Total Gold Particles per Dendrite Area (#/µm²)	Number (%) Gold Particles on Membrane	Number (%) Intracellular Gold Particles	Number eGFP-D2R Labeled Spines	Total Gold Particles per Spine Area (#/µm²)	Number (%) Gold Particles on Membrane	Number (%) Intracellular Gold Particles
1	94	74	10.14	368 58%	269 42%	20	37.26	73 89%	9 11%
2	86	94	9.98	381 66%	194 34%	14	37.59	44 77%	13 23%
3	39	86	12.36	119 59%	84 41%	10	25.79	28 90%	3 10%
4	71	39	8.64	214 69%	95 31%	16	21.84	48 75%	16 25%
5	14	71	5.96	34 49%	36 51%	1	20.26	2 100%	0 0%
6	33	14	9.68	139 63%	81 37%	5	26.61	10 67%	5 33%
7	62	33	12.42	312 82%	70 18%	11	29.87	35 97%	1 3%
8	14	62	8.40	51 44%	65 56%	0	-	-	-
N **mean** **sem**	413	14	9.70 0.75	**61%**	**39%**	77	28.46 2.60	**85%**	**15%**

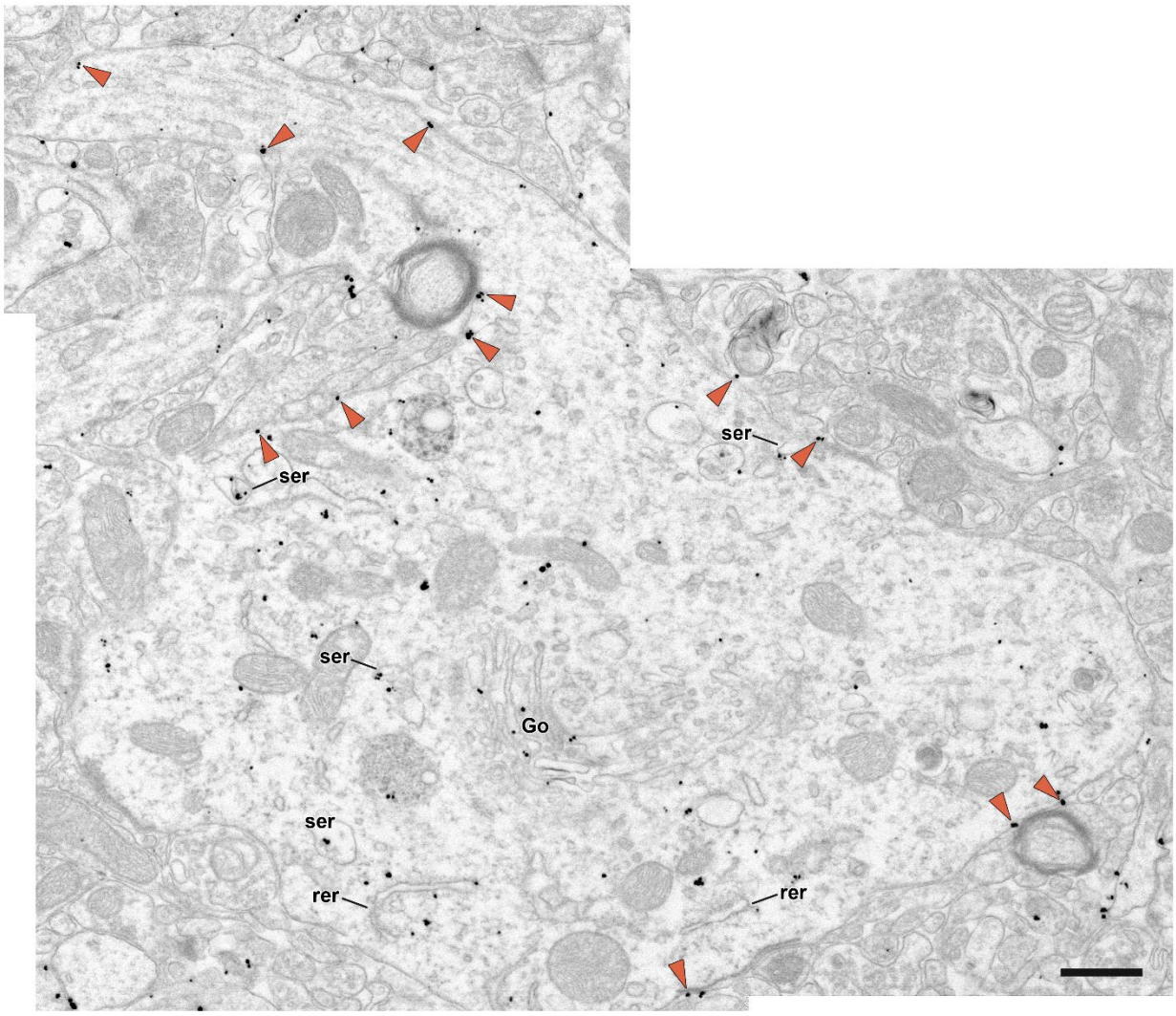

Figure 12: Electron micrograph montage showing an eGFP-D2R immunogold labeled distal dendrite branching off of a proximal dendrite in the mouse Str

Immunogold labeling is contained mainly intracellularly, but the proportion of immunogold bound to the membrane (orange arrowheads) increases in the direction of a more distal dendritic branch (upper left). Similar to immunopositive dendrites in the SNc, intracellular immunogold particles are associated with the rough endoplasmic reticulum (rer), smooth endoplasmic reticulum (ser), and Golgi apparatus (Go). Scale bar 0.6 µm.

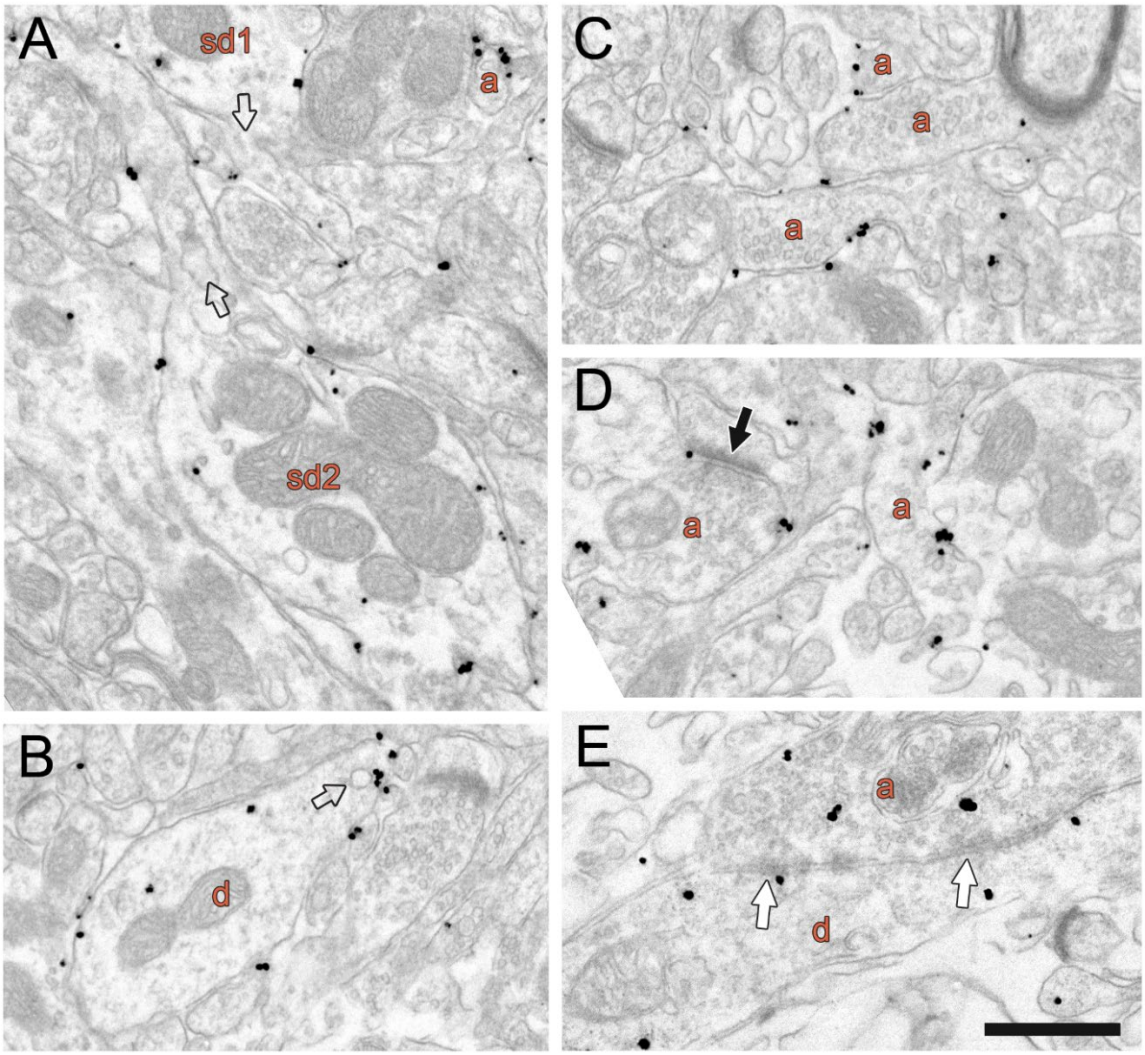

Figure 13: Electron micrographs of eGFP-D2R immunogold labeled dendrites, spiny dendrites, and axon terminals in the mouse Str

(**A**) Two spiny dendrites (sd1 and sd2) contain eGFP-D2R immunogold that is mainly present on the membrane of both the dendrites and the necks of their spines (transparent arrows). (**B**) A dendritic profile (d) appears to exhibit the same expression of membrane-bound D2R, with a collection of immunogold found on the membrane of what may be the proximal neck of a spine (transparent arrow). (**C-E**) eGFP-D2r immunogold is observed mainly on the membranes of axon terminals (a) that are identified by concentrations of small clear synaptic vesicles. Single-section imaging shows that many of these axon terminals do not form synapses in single sections, although some terminals do form either asymmetric (black arrow) or symmetric synapses (white arrows) with nearby dendrites and spines. Scale bar 0.6 µm.

Table 8: Distribution of eGFP-D2R Gold Particles within Axon Terminals of the Mouse Str

Mouse	Number eGFP-D2R Labeled Terminals	Average Terminal Area (μm^2)	Total Gold Particles per Terminal Area (#/μm^2)	Average Terminal Perimeter (μm)	Membrane Gold Particles per Terminal Perimeter (#/μm)	Number (%) Gold Particles on Membrane	Number (%) Intracellular Gold Particles	Synapses Formed by Axons		
								Symmetric	Asymmetric	None
1	31	0.40	14.21	3.42	0.67	86 67%	43 33%	1	7	23
2	23	0.19	26.80	2.23	0.65	60 65%	32 35%	0	2	21
3	9	0.26	15.92	2.63	0.72	23 72%	9 28%	0	1	8
4	19	0.44	13.25	3.24	0.76	60 76%	19 24%	0	3	16
5	1	0.30	9.86	2.02	1.00	3 100%	0 0%	0	0	1
6	9	0.39	17.23	3.51	0.65	35 65%	19 35%	1	0	8
7	19	0.42	12.31	2.52	0.79	52 79%	14 21%	0	5	14
8	8	0.97	7.54	4.41	0.36	16 36%	28 64%	3	1	4
N **mean** **sem**	119	0.42 0.08	14.64 2.06	3.00 0.28	0.70 0.06	**70%**	**30%**	5 4%	19 16%	95 80%

4.0 Discussion

The primary objective of this study was to provide anatomical information about D2 autoreceptor localization as it relates to the understanding of dendrodendritic DA transmission in the SNc. Immunogold labeling in transgenically modified mice expressing an exogenous eGFG-tag on the D2R appeared to reveal the location of a greater number of D2Rs than previously observed by electron microscopy. In the dendrites and axon terminals of the SNc, eGFP-D2R immunogold was more often found internally associated with the ser than bound to the plasma membrane. In dendrites of both the SNc and the Str, the proportion of membrane-bound eGFP-D2R increased as profile diameter decreased, reflective of distal location. eGFP-D2R immunogold particles on the SNc dendritic membranes were spread out and rarely directly apposed to other dendrites. A higher expression of both total and membrane-bound eGFP-D2R was observed in the Str relative to the SNc. A novel site for eGFP-D2R was discovered on the AIS of SNc neurons, where immunogold particles were found both on and near (~40 nm) the membrane. The dispersed distribution of D2R labeling on the plasma membrane has functional implications for understanding the nature of DA transmission in the SNc (Fig. 14).

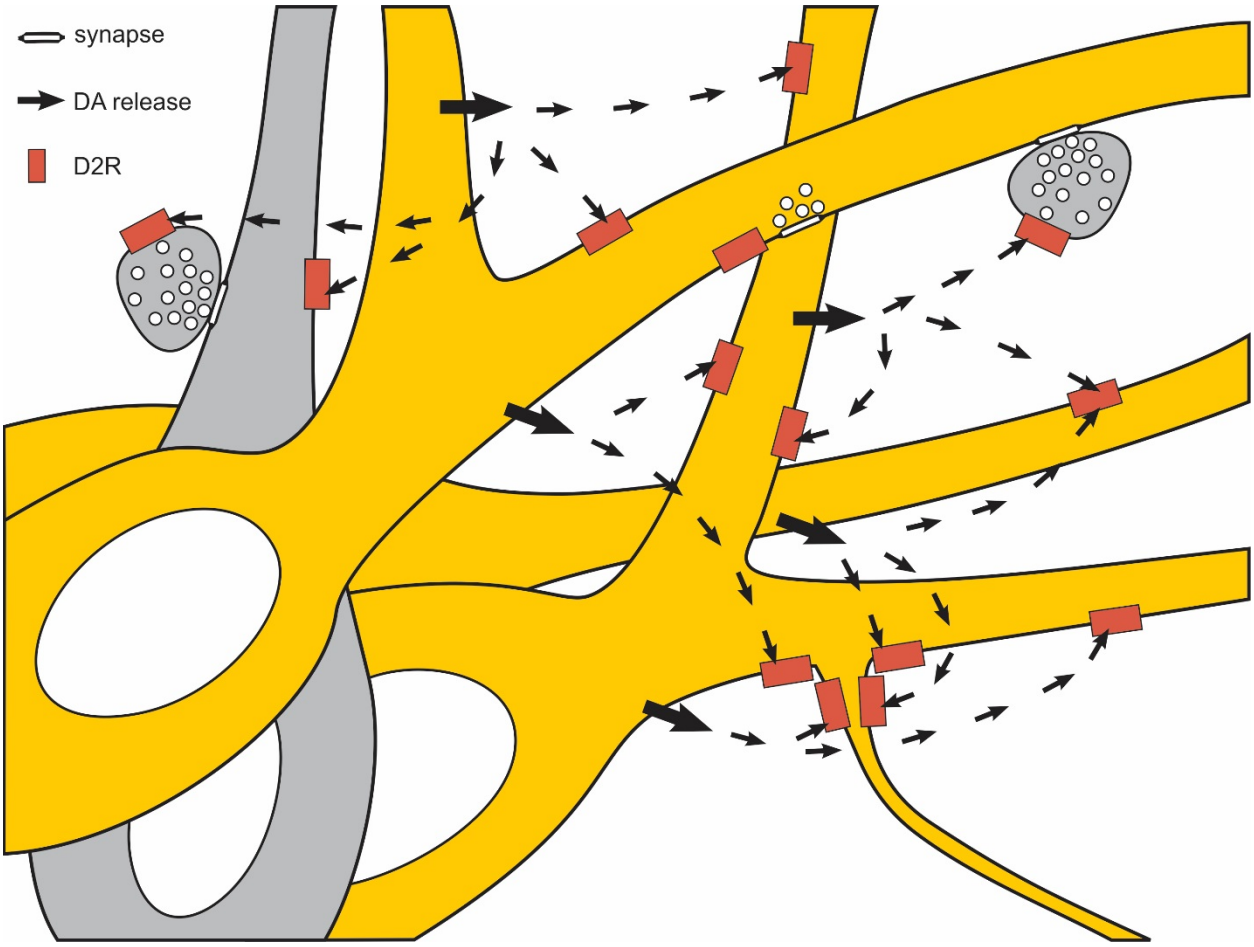

Figure 14: Schematic drawing of possible volume transmission of DA through the SNc

Immunogold labeling suggests the presence of randomly spread D2R (orange rectanges) along the dendritic membranes of presumed DA cells (yellow cells) and possibly some non-DA cells (gray cell). D2Rs probably also function on the membranes of non-DA axon terminals in the SNc (round structures filled with white vesicles), where they modulate the release of neurotransmitters. Some DA may transmit intercellularly through traditional dendrodendritic synapses, but the majority of somatodendritically released DA appears to travel some distance in order to active D2Rs. A novel observation of eGFP-D2R immunogold seen on the membrane of axon initial segments indicates that D2R on the AIS (bottom right emenating process) may serve a distinct function.

4.1 Methodological Limitations

Our examination of immunogold labeling of eGFP-D2R replicated much of the existing literature on the cellular and subcellular location of D2R in both the midbrain and the Str (Garzon et al 2013, Hersch et al 1995, Pickel et al 2002, Sesack et al 1994, Wang & Pickel 2002, Yung & Bolam 2000, Yung et al 1995). The continuity between the results described in the present paper and the observations of previous studies, regardless whether they used more sensitive labeling techniques (Hersch et al 1995, Pickel et al 2002, Sesack et al 1994, Wang & Pickel 2002, Yung & Bolam 2000) or an approach emphasizing subcellular resolution (Garzon et al 2013, Hersch et al 1995), indicates the overall soundness of the present methodology. Nevertheless, there are always ways in which scientific investigations are limited by their procedures.

The most significant limitation of our approach is the one inherent in all immunohistochemical electron microscopic analyses, and that is the constant likelihood of false negative outcomes. The process of fixing proteins and lipids in tissue in preparation for viewing in the electron microscope prevents a substantial number of antibodies from deeply penetrating the tissue. Solubilizing membranes with detergent would increase antibody penetration, but this must be kept to a minimum in ultrastructural studies so that fine structures can remain intact. There is also a limited sensitivity of the immunogold labeling technique that was used to identify D2Rs. Other methods, such as immunoperoxidase, result in greater signal but are unable to reveal the exact subcellular localization of antigens that was required for this study (Sesack et al 2006). To a certain extent, the transgenic incorporation of a protein tag on the D2R appeared to mitigate these concerns by increasing overall immunogold signal and therefore providing a better estimate of receptor expression than previously available. Still, this study can only provide an estimate of D2R

localization rather than ground truth, and our findings must be interpreted as an underestimate in all analyzed locations.

It was not appreciated until the analysis was complete that variation in gold particle size could impact estimation of individual particle association with the plasma membrane or organelles. This is because the 20 nm criterion was applied between the membrane and the edge of the silver-enhanced gold particles. Consequently, larger particles close to the membrane had a greater chance of being characterized as membrane-associated than smaller particles. On the whole, variation in the levels of silver enhancement with the Aurion product used in the present study was less marked than with previously employed methods (Chan et al 1990, Sesack et al 2006). Furthermore, the majority of gold particles were unequivocally localized intracellularly or associated with the plasma membrane or organelles. Hence, we do not feel that this issue unduly affected the results. Nevertheless, to avoid the problem posed by variable particle size, subsequent studies will be conducted using a criterion of 20 nm between the membrane and the center of silver-enhanced gold particles.

Despite the general underestimation of the D2R in this study and variation in gold particle size, statistical comparisons between the SNc and the Str showed that significant differences in the density of D2R expression between various brain regions were detectable. The greater overall D2R signal in the Str indicates that the eGFP tag-enhanced immunogold method had the capacity to distinguish greater receptor concentration where it was present. Differences in the numbers of membrane-bound eGFP-D2R immunogold labeling also indicated that the density of D2 autoreceptors on the dendritic membrane of SNc cells is substantially lower than the expression of post-synaptic D2 receptors in the Str.

It was initially hoped that the increased D2R detection sensitivity from the inclusion of the eGFP tag might also reveal D2R presence immediately inside DA synapses in the Str. Comprehensive analysis of immunogold-labeling in this area, however, showed no such case, indicating a possible absence of receptors in the immediate post-synaptic region. Alternatively, this observation could reflect a limitation of the pre-embedding method, which exposes tissue to antibodies before ultrathin sectioning (Sesack et al 2006). The alternative post-embedding method involves ultrathin sectioning of tissue before antibody exposure, which theoretically increases antibody penetration into synapses and other dense protein complexes (Sesack et al 2006, Somogyi et al 1998). Despite the methodological limitations mentioned, our observations corroborated existing reports that also failed to observe D2R within synapses of either the midbrain or the Str (Garzon et al 2013, Yung et al 1995).

Another limitation of this study involved incomplete sampling of the SNc from the mouse brain. Sectioning and trimming of brain tissue isolated an area of the SNc that was in the middle of both medio-lateral and rostro-caudal dimensions, and we did not explore other parts of the structure. While the SNc is one of the more homogenous regions of the DA system, differences between sub-regions in the structure have been identified. Previous studies have described dorsal and ventral tiers of the SNc, which project to different regions of the Str (Bjorklund & Dunnett 2007, Fallon & Loughlin 1995, Gerfen et al 1987). There are also differences in the types of calcium-binding proteins expressed by cells throughout the midbrain that extend beyond the simple dorsal/ventral tier distinctions (Nemoto et al 1999). This implies that D2R expression and function might differ in the various sub-regions of the SNc. In lieu of more inclusive studies, the findings of the present paper should therefore be interpreted solely as a first approximation of the nigral area.

4.2 Intracellular D2R

Immunogold labeling indicated that the majority of D2R in dendrites of DA cells in the SNc are not bound to the membrane. Instead, they are located internally, associated with Golgi bodies, multivesicular bodies, and both forms of endoplasmic reticulum, observations that have been made previously (Garzon et al 2013, Pickel et al 2002, Sesack et al 1994). Intracellular DA receptors perform no known function when not bound to the membrane, and so their common intracellular presence prompts consideration.

All G-protein coupled receptors are made in the rough endoplasmic reticulum and then transferred to the Golgi complex where they undergo modifications. From the Golgi, these receptors must be transferred to their functional positions on the cell membrane. Little is known about the exact mechanisms that correctly traffic DA receptors from the Golgi to the plasma membrane, although the process is heavily regulated (Duvernay et al 2005, Free et al 2007, Young et al 2015). The intracellular organelle most consistently found to express D2R-immunogold, namely the ser, represents a potential trafficking mechanism for this receptor. Previous studies have shown that the ser is involved in many cases of non-vesicular receptor transportation and storage in dendrites (Ramirez & Couve 2011). Furthermore, when D2R chaperone-assisted movement to the membrane has been prevented, the result has been retention of the receptor within the ser (Free et al 2007, Prou et al 2001). Despite the strength of this circumstantial evidence, direct proof is still required to demonstrate that newly-synthesized DA receptors utilize the continuous ser as a corridor through which they can travel throughout the neuron.

The presence of D2R labeling in multivesicular bodies is probably explained by the organelle's function in membrane protein degradation. As with many membrane-associated proteins, DA receptors require continuous turnover. They are therefore endocytosed from the

membrane and packaged into multivesicular bodies for transport to lysosomes (Piper & Katzmann 2007). There, the proteins are destroyed, and their components are recycled. Throughout this process, eGFP-tags that are presumably still intact enough for antibody-recognition could be detected by immunogold labeling.

4.3 D2R Modification of Neuronal Firing at the Axon Initial Segment

Throughout the course of analyzing D2R in the SNc, immunolabeling was unexpectedly found both intracellularly and on the plasma membrane of presumed AISs. Classifying these profiles as AISs was suggested by their dense submembrane undercoating, enlarged surrounding extracellular space, and occasional expression of extracellular granules, all of which are distinguishing characteristics of the AIS in other cell types (Kosaka 1980, Peters et al 1968). The absence of visible synaptic input to these profiles is a trait that has been described specifically for the AIS of SNc DA cells, and their size also corresponds to the diameter (0.2-0.8 μm) typically reported for the DA cell AIS (Gonzalez-Cabrera et al 2017).

The preliminary observation of eGFP-D2R colocalization with beta IV-spectrin also is consistent with localization of the D2R at the AIS of SNc neurons. This protein, along with ankyrin-G, composes a protein complex that distinguishes the AIS from the rest of the neuron (Leterrier 2016). This “scaffolding” complex lies just under the plasma membrane and is found only at the AIS and nodes/paranodes of Ranvier, a spatial restriction that was confirmed for beta IV-spectrin immunoreactivity in the present study. The cells with D2R-expressing AISs are presumed to be DA neurons, given that the vast majority of cells in the SNc are dopaminergic (van der Kooy et al 1981) and that mRNA for the D2R is expressed almost exclusively by DA neurons

(Le Moine & Bloch 1991). Beyond this assumption, the presence of D2R on the AIS of DA cells in the SNc has been directly confirmed by triple immunolabeling for TH, ankyrin-G, and eGFP-D2R as performed by our colleague John Williams (unpublished observations).

Besides the typical intracellular and membrane-associated eGFP-D2R immunogold at the AIS, the additional gold particles found ~40 nm from the plasma membrane seem to be too deep to indicate functional receptors. Still, their common and peculiar placement prompts some functional speculation. One of the known functions of the AIS scaffolding is the bundling of microtubules to facilitate vesicular transport to and from the axon (Leterrier 2016). The immunogold's close proximity to the AIS scaffolding, sometimes visible just under the dense membrane undercoating, may indicate that D2Rs are trafficked along organized microtubules through the interior of the AIS. Indeed, the AIS scaffolding is known to selectively facilitate the movement of axonal membrane proteins through vesicular transport along microtubules while filtering out and removing cargo that must remain in the somatodendritic complex (Leterrier 2018). Because D2Rs are found throughout both major cellular compartments, however, it is unclear how much sorting they actually require. Furthermore, most research investigating trafficking of DA receptors indicates the importance of the ser (see section 4.2), through which D2Rs may bypass the AIS sorting compartment. It is challenging to provide any further ideas about the purpose of the D2R labeling ~40 nm from the AIS plasma membrane, other than to speculate that it might represent some form of receptor awaiting rapid deployment to the membrane. Evidence to support such a supposition will require the means for directly observing D2R movements at the AIS in a functional preparation.

Although D2-like receptors have been described at the AIS in other brain regions (see below), our findings mark the first report of the D2R being present specifically as an autoreceptor

at the AIS of presumed SNc DA neurons. The prospect of D2Rs being functionally active at this site is of prime importance, given the central role of the AIS in determining neuronal firing. Identification of the AIS as the site of action potential generation has been linked to the high concentration of voltage-gated sodium and potassium channels along this part of the membrane (Leterrier 2016). Indeed, ankyrin-G is necessary for the accumulation of the sodium channels and the designation of this neuronal compartment as axonal (Hedstrom et al 2008). In the SNc, the AIS of DA cells is the site of generation for spontaneous firing (Grace & Bunney 1983b), and its length is a direct determinant of firing rate (Meza et al 2018). The location of the AIS on these neurons is somewhat atypical, as it branches off of a major dendrite (Gonzalez-Cabrera et al 2017, Grace & Bunney 1983b), and this displacement from the soma has significant implications for neuronal firing. For example, the AIS may have an increased sensitivity to inputs that synapse onto the axon-bearing dendrite (Leterrier 2016). Additionally, the slow oscillation of the AIS must combine with a second oscillator within the somatodendritic complex of DA cells to create a compromise coupled-oscillator in the determination of final firing rate (Meza et al 2018).

A possible role for DA receptor functioning on the AIS has been described in studies of the GABAergic cartwheel neurons of the dorsal cochlear nucleus, which, like SNc DA cells, exhibit both tonic and burst firing patterns (Bender et al 2010). On the AIS of these neurons, the DA receptor subtype D3R is activated by endogenously released DA. Through β-arrestin-dependent signaling and its subsequent activation of phosphokinase C, the voltage-gated Cav3.2 calcium channel is modulated (Bender et al 2010, Bender et al 2012, Yang et al 2016). This channel alteration reduces Ca2+ influx into the AIS, decreasing spiking (Bender et al 2010) and transforming bursting cells into tonically firing ones (Bender et al 2012). It is unknown whether SNc DA cells also undergo this mechanism of DA modulation at the AIS. Previous research

suggests that it is the D3 DA receptor that acts on dorsal cochlear nucleus interneurons, whereas the D3R does not function as an autoreceptor in the SNc (Koeltzow et al 1998, Mercuri et al 1997). Additionally, the presence of the related Cav3.2 channel subtype has not yet been shown on the AIS of SNc DA cells.

The effect of DA when released specifically onto the AIS of SNc DA cells has not been tested. There has been one study, however, of DA's effect on D2Rs along the soma/axon-bearing dendrite/AIS region of DA neurons extending into the SNr, although the authors could not have known that D2Rs were also present on the AIS (Gentet & Williams 2007). Application of DA onto the somatic area of these SNr DA neurons decreased the frequency at which action potentials backpropagated from the AIS into the somatodendritic complex. This effect was interpreted as being caused by the activation of D2Rs on the soma but could have occurred due to receptors on the AIS as well. In either case (or both), D2R-mediated hyperpolarization of the membrane then altered the availability of voltage-gated sodium and potassium channels that isolated the action potential to the AIS and axon-bearing dendrite (Gentet & Williams 2007).

In the intact SNc, whether or not action potentials generated at the AIS become confined to the axon-bearing dendrite or backpropagate throughout the somatodendritic compartment may reflect a balance between the autoregulatory effects of the D2Rs and the density of excitatory and inhibitory synapses on the dendrite from which the axon emanates. In hippocampal oriens-alveus interneurons, which also have an AIS that branches off of a major dendrite, high intensity stimulation reportedly shifts the site of action potential generation from the AIS to the somatodendritic compartment, reflecting an altered availability of voltage-gated ion channels along the AIS-region (Martina et al 2000). These hippocampal interneurons do not exhibit the spontaneous firing patterns of SNc DA cells and differ from them in other fundamental ways,

making it difficult to extrapolate further from their physiological properties. Nevertheless, future studies should be directed towards investigating how the density of excitatory and inhibitory synapses compares between the axon-bearing dendrite and the other dendrites of DA SNc neurons.

4.4 Insight into Dendrodendritic DA Autoregulation

The present investigation was primarily driven by an interest in the mechanisms of neuronal DA communication in the SNc. DA transmission between cells is known to rarely involve dendrodendritic synapses in the midbrain (Bayer & Pickel 1990, Groves & Linder 1983), an observation we corroborated in the present study. Consequently, intercellular DA communication via D2 autoreceptors in the SNc and VTA must be non-conventional. With this in mind, two basic possibilities of non-canonical DA transmission arise. Either the sites of DA release and receipt are located in close contact with one another but do not form familiar structural junctions, or these communicating components are separated by some real distance. The former view of non-traditional "synaptic" transmission has been suggested by our colleague, John Williams, in his publications (described below; see also (Ford 2014)), while the latter scenario is more commonly referred to as extrasynaptic or volume transmission (Agnati et al 1992).

Multiple arguments regarding the former hypothesized mode of communication have been based on electrophysiological studies. Temporal analysis of DA-evoked IPSCs in the VTA have suggested that D2R activation requires a highly concentrated amount of DA released in a relatively short amount of time, corresponding to the release that would be present in a synaptic cleft (Beckstead et al 2004, Ford et al 2009). In this regard, it is interesting to note that the tubulovesicles likely to contain and release DA from dendrites in the SNc and VTA are substantially larger than

traditional synaptic vesicles (Nirenberg et al 1996). Further evidence comes from electrical stimulation studies showing a constant onset latency of D2R-IPSCs across stimulus intensity, suggesting that distant release sites did not drop out as stimulus amplitude declined (Beckstead et al 2004). Furthermore, iontophoresis of DA onto VTA cells, which requires diffusion to reach the D2R, could not reproduce the speed with which endogenously released DA was able to transmit to neighboring dendrites (Beckstead et al 2004). Additionally, application of dextran to slow diffusion through the extracellular space did not affect the onset latency of evoked D2R-IPSCs, while it did delay the response to ionotophoretic DA (Ford et al 2010). These observations suggest that DA is transmitted through a non-traditional "synaptic" mechanism that has yet to be defined.

Anatomical observations from the present study, however, do not lend credence to this theory of non-canonical synaptic transmission, given that only 7% of membrane-bound D2R immunogold particles on SNc dendrites were directly apposed to other dendrites. The finding that most membrane associated D2Rs were adjacent to axon terminals or glia suggests that the autoreceptor is more likely to bind DA that is diffusing in the extracellular space and, therefore, that some distance must exist between dendritic DA release and dendritic receipt by D2Rs.

Based on the anatomical observations of dispersed membrane-bound D2R on SNc dendrites, it is more likely that the transmission of DA in this area aligns with the theory of volume transmission, as described previously (Agnati et al 1992, Rice 2000). Studies of extracellular DA concentration in the SNc show that movement of DA through the extracellular space is minimally impacted by uptake via the dopamine transporter (DAT) (Cragg & Rice 2004). Anatomical research corroborates this finding, showing that DAT is found less frequently on the membrane of SNc dendrites as compared to axons (Block et al 2015, Nirenberg et al 1996). This negligible DA uptake allows diffusion to be the primary limiter of DA movement through the extracellular space,

causing the neurochemical to reach further distances in the SNc than it can in the Str (Rice & Cragg 2008). Based on direct measurements and modeling, it has been theorized that quantal release of DA from SNc dendrites can activate D2R up to 8 μm away from a point source (Rice & Cragg 2008). This diffusion then is likely to account for the activation of most membrane-bound D2Rs that have no clear proximity to DA dendrites that could serve as release sites.

The rather marked differences in conclusions that have been made between electrophysiologically recorded D2R-IPSCs and neurochemically-measured extracellular DA concentrations have prompted a re-analysis of the studies estimating the time course of DA transmission in the midbrain (Rice & Patel 2015). Of the total time that it takes for electrically-evoked dendritic DA release to evoke an IPSC on another dendrite, the majority of this time is occupied by the kinetics of the D2R-activated GIRK potassium channel (Ford et al 2009). The extracellular DA concentration has been found to reach its peak around 10 ms after evoked dendritic release, but the eventual GIRK-facilitated IPSC occurs several hundred milliseconds afterwards (Rice & Patel 2015). This disparity has suggested that the method of recording D2R-IPSC timing may not provide an accurate reflection of the time course of inter-dendritic DA transmission through the extracellular space (Rice & Patel 2015).

Even if SNc DA neurons communicate with one another through a volume transmission mode, it might still be efficient for the cell to dedicate particular regions of the membrane for receipt of autoreceptor signals. In this case, areas of dense dendritic membrane-bound D2R expression might be expected in so-called “hot spots.” Few instances of concentrated eGFP-D2R immunogold were observed in our study, however, and none of them continued in multiple serial sections. Collectively, the results of this study are more consistent with membrane-bound D2Rs being spread fairly evenly throughout the dendritic tree, although it must be noted that the

stoichiometry of immunogold labeling is not known, i.e., it is unknown how many D2Rs are represented by one silver-enhanced gold particle. On the whole, D2Rs are more likely to be associated with the membrane in distal than proximal dendrites and when present in the AIS. Hence, if there is any component specialization, these two compartments of SNc DA neurons appear to be the most specialized for receipt of D2 autoreceptor signals.

Concerning DA transmission as a whole, the results of the present investigation are primarily reflective of dendritic DA receipt and not of release. The reported lack of definitive clustering of membrane-bound D2Rs adjacent to dendrites may suggest that the somatodendritic sites of DA release are similarly dispersed. Some evidence has been presented that SNc DA cells have the capacity to release DA outside of active zones, although so far this has been shown only in the axonal and not the dendritic region (Liu et al 2018). Knowing that vesicles are fusion-competent even in the absence of active zones (Wang et al 2016) makes it important to reconsider whether there is any region of the DA dendritic membrane that is specialized for release or whether such events can occur at any site where there are reserpine-sensitive tubulovesicles (Nirenberg et al 1996) and sufficient accumulated Ca2+. The consistent finding of spontaneous D2R-mediated IPSCs recorded in SNc dendrites (Gantz et al 2013) may simply reflect the responses of diffusely-positioned D2Rs to diffusely-arranged DA release sites.

5.0 Conclusions

This study was the first to use electron microscopy to observe the subcellular location of D2 autoreceptors in the SNc utilizing a new mouse model containing an exogenous tag on the D2R. This method qualitatively enhanced overall D2R signal, revealing the location and density of these receptors that is closer to actuality. Concerns about low immunogold signaling on dendritic membranes in the SNc were offset by findings of higher levels of labeling on Str membranes, which further suggested that relative amounts of labeling observed were at least correlated with physiological expression levels. The observation that most dendritic membrane-bound eGFP-D2R labeling in the SNc was not directly apposed to neighboring dendrites supports the volume transmission mode of DA communication. Distal dendrites and their greater proportion of membrane D2R may provide specialized sites for DA receipt, accompanied by an increased expression of D2R on the AIS membrane, mediating a new form of autoinhibition.

Future research should explore more precise methodology for analyzing actual D2R expression in the SNc as well as possible mechanisms for DA to be released from the somatodendritic complex. This may lead to a better understanding of how much distance actually exists between DA release and receipt, furthering the understanding of how DA is used as a communication signal in this area. Additionally, future studies should investigate the possible role of DA activating D2 autoreceptors on the AIS and the exact cellular mechanisms through which these receptors affect neuronal activity.

6.0 Bibliography

Agnati LF, Bjelke B, Fuxe K. 1992. Volume Transmission in the Brain. *American Scientist* 80: 362-73

Bamford NS, Zhang H, Schmitz Y, Wu NP, Cepeda C, et al. 2004. Heterosynaptic dopamine neurotransmission selects sets of corticostriatal terminals. *Neuron* 42: 653-63

Bayer VE, Pickel VM. 1990. Ultrastructural localization of tyrosine hydroxylase in the rat ventral tegmental area: relationship between immunolabeling density and neuronal associations. *J Neurosci* 10: 2996-3013

Beckstead MJ, Grandy DK, Wickman K, Williams JT. 2004. Vesicular dopamine release elicits an inhibitory postsynaptic current in midbrain dopamine neurons. *Neuron* 42: 939-46

Bello EP, Mateo Y, Gelman DM, Noain D, Shin JH, et al. 2011. Cocaine supersensitivity and enhanced motivation for reward in mice lacking dopamine D2 autoreceptors. *Nat Neurosci* 14: 1033-8

Bender KJ, Ford CP, Trussell LO. 2010. Dopaminergic modulation of axon initial segment calcium channels regulates action potential initiation. *Neuron* 68: 500-11

Bender KJ, Uebele VN, Renger JJ, Trussell LO. 2012. Control of firing patterns through modulation of axon initial segment T-type calcium channels. *J Physiol* 590: 109-18

Bjorklund A, Dunnett SB. 2007. Dopamine neuron systems in the brain: an update. *Trends Neurosci* 30: 194-202

Block ER, Nuttle J, Balcita-Pedicino JJ, Caltagarone J, Watkins SC, et al. 2015. Brain Region-Specific Trafficking of the Dopamine Transporter. *J Neurosci* 35: 12845-58

Borroto-Escuela DO, Perez De La Mora M, Manger P, Narvaez M, Beggiato S, et al. 2018. Brain Dopamine Transmission in Health and Parkinson's Disease: Modulation of Synaptic Transmission and Plasticity Through Volume Transmission and Dopamine Heteroreceptors. *Front Synaptic Neurosci* 10: 20

Bourdy R, Sanchez-Catalan MJ, Kaufling J, Balcita-Pedicino JJ, Freund-Mercier MJ, et al. 2014. Control of the nigrostriatal dopamine neuron activity and motor function by the tail of the ventral tegmental area. *Neuropsychopharmacology* 39: 2788-98

Bouyer JJ, Park DH, Joh TH, Pickel VM. 1984. Chemical and structural analysis of the relation between cortical inputs and tyrosine hydroxylase-containing terminals in rat neostriatum. *Brain Res* 302: 267-75

Celada P, Paladini CA, Tepper JM. 1999. GABAergic control of rat substantia nigra dopaminergic neurons: role of globus pallidus and substantia nigra pars reticulata. *Neuroscience* 89: 813-25

Cepeda C, Buchwald NA, Levine MS. 1993. Neuromodulatory actions of dopamine in the neostriatum are dependent upon the excitatory amino acid receptor subtypes activated. *Proc Natl Acad Sci U S A* 90: 9576-80

Chan J, Aoki C, Pickel VM. 1990. Optimization of differential immunogold-silver and peroxidase labeling with maintenance of ultrastructure in brain sections before plastic embedding. *J Neurosci Methods* 33: 113-27

Chen BT, Patel JC, Moran KA, Rice ME. 2011. Differential calcium dependence of axonal versus somatodendritic dopamine release, with characteristics of both in the ventral tegmental area. *Front Syst Neurosci* 5: 39

Courtney NA, Ford CP. 2014. The timing of dopamine- and noradrenaline-mediated transmission reflects underlying differences in the extent of spillover and pooling. *J Neurosci* 34: 7645-56

Cragg SJ, Greenfield SA. 1997. Differential autoreceptor control of somatodendritic and axon terminal dopamine release in substantia nigra, ventral tegmental area, and striatum. *J Neurosci* 17: 5738-46

Cragg SJ, Rice ME. 2004. DAncing past the DAT at a DA synapse. *Trends Neurosci* 27: 270-7

David HN, Ansseau M, Abraini JH. 2005. Dopamine-glutamate reciprocal modulation of release and motor responses in the rat caudate-putamen and nucleus accumbens of "intact" animals. *Brain Res Brain Res Rev* 50: 336-60

Descarries L, Watkins KC, Garcia S, Bosler O, Doucet G. 1996. Dual character, asynaptic and synaptic, of the dopamine innervation in adult rat neostriatum: a quantitative autoradiographic and immunocytochemical analysis. *J Comp Neurol* 375: 167-86

Dube L, Smith AD, Bolam JP. 1988. Identification of synaptic terminals of thalamic or cortical origin in contact with distinct medium-size spiny neurons in the rat neostriatum. *J Comp Neurol* 267: 455-71

Dunlop BW, Nemeroff CB. 2007. The role of dopamine in the pathophysiology of depression. *Arch Gen Psychiatry* 64: 327-37

Duvernay MT, Filipeanu CM, Wu G. 2005. The regulatory mechanisms of export trafficking of G protein-coupled receptors. *Cell Signal* 17: 1457-65

Fahn S. 2015. The medical treatment of Parkinson disease from James Parkinson to George Cotzias. *Mov Disord* 30: 4-18

Fallon JH, Loughlin SE. 1995. Substantia Nigra In *The Rat Nervous System*, ed. G Paxinos. San Diego, California: Academi Press, Inc.

Farnebo LO, Hamberger B. 1971. Drug-induced changes in the release of 3 H-monoamines from field stimulated rat brain slices. *Acta Physiol Scand Suppl* 371: 35-44

Ferron A, Thierry AM, Le Douarin C, Glowinski J. 1984. Inhibitory influence of the mesocortical dopaminergic system on spontaneous activity or excitatory response induced from the thalamic mediodorsal nucleus in the rat medial prefrontal cortex. *Brain Res* 302: 257-65

Floresco SB, West AR, Ash B, Moore H, Grace AA. 2003. Afferent modulation of dopamine neuron firing differentially regulates tonic and phasic dopamine transmission. *Nat Neurosci* 6: 968-73

Ford CP. 2014. The role of D2-autoreceptors in regulating dopamine neuron activity and transmission. *Neuroscience* 282: 13-22

Ford CP, Gantz SC, Phillips PE, Williams JT. 2010. Control of extracellular dopamine at dendrite and axon terminals. *J Neurosci* 30: 6975-83

Ford CP, Phillips PE, Williams JT. 2009. The time course of dopamine transmission in the ventral tegmental area. *J Neurosci* 29: 13344-52

Free RB, Hazelwood LA, Cabrera DM, Spalding HN, Namkung Y, et al. 2007. D1 and D2 dopamine receptor expression is regulated by direct interaction with the chaperone protein calnexin. *J Biol Chem* 282: 21285-300

Freeman AS, Meltzer LT, Bunney BS. 1985. Firing properties of substantia nigra dopaminergic neurons in freely moving rats. *Life Sci* 36: 1983-94

Gantz SC, Bunzow JR, Williams JT. 2013. Spontaneous inhibitory synaptic currents mediated by a G protein-coupled receptor. *Neuron* 78: 807-12

Garzon M, Duffy AM, Chan J, Lynch MK, Mackie K, Pickel VM. 2013. Dopamine D(2) and acetylcholine alpha7 nicotinic receptors have subcellular distributions favoring mediation of convergent signaling in the mouse ventral tegmental area. *Neuroscience* 252: 126-43

Gauthier J, Parent M, Levesque M, Parent A. 1999. The axonal arborization of single nigrostriatal neurons in rats. *Brain Res* 834: 228-32

Gentet LJ, Williams SR. 2007. Dopamine gates action potential backpropagation in midbrain dopaminergic neurons. *J Neurosci* 27: 1892-901

Gentry RN, Schuweiler DR, Roesch MR. 2018. Dopamine signals related to appetitive and aversive events in paradigms that manipulate reward and avoidability. *Brain Res* [Epub ahead of print]

Gerfen CR, Herkenham M, Thibault J. 1987. The neostriatal mosaic: II. Patch- and matrix-directed mesostriatal dopaminergic and non-dopaminergic systems. *J Neurosci* 7: 3915-34

Gonon FG, Buda MJ. 1985. Regulation of dopamine release by impulse flow and by autoreceptors as studied by in vivo voltammetry in the rat striatum. *Neuroscience* 14: 765-74

Gonzalez-Cabrera C, Meza R, Ulloa L, Merino-Sepulveda P, Luco V, et al. 2017. Characterization of the axon initial segment of mice substantia nigra dopaminergic neurons. *J Comp Neurol* 525: 3529-42

Grace AA. 1990. Evidence for the functional compartmentalization of spike generating regions of rat midbrain dopamine neurons recorded in vitro. *Brain Res* 524: 31-41

Grace AA. 2016. Dysregulation of the dopamine system in the pathophysiology of schizophrenia and depression. *Nat Rev Neurosci* 17: 524-32

Grace AA, Bunney BS. 1983a. Intracellular and extracellular electrophysiology of nigral dopaminergic neurons--1. Identification and characterization. *Neuroscience* 10: 301-15

Grace AA, Bunney BS. 1983b. Intracellular and extracellular electrophysiology of nigral dopaminergic neurons--2. Action potential generating mechanisms and morphological correlates. *Neuroscience* 10: 317-31

Grace AA, Bunney BS. 1983c. Intracellular and extracellular electrophysiology of nigral dopaminergic neurons--3. Evidence for electrotonic coupling. *Neuroscience* 10: 333-48

Groves PM, Linder JC. 1983. Dendro-dendritic synapses in substantia nigra: descriptions based on analysis of serial sections. *Exp Brain Res* 49: 209-17

Hedstrom KL, Ogawa Y, Rasband MN. 2008. AnkyrinG is required for maintenance of the axon initial segment and neuronal polarity. *J Cell Biol* 183: 635-40

Hersch SM, Ciliax BJ, Gutekunst CA, Rees HD, Heilman CJ, et al. 1995. Electron microscopic analysis of D1 and D2 dopamine receptor proteins in the dorsal striatum and their synaptic relationships with motor corticostriatal afferents. *J Neurosci* 15: 5222-37

Hirata K, Yim CY, Mogenson GJ. 1984. Excitatory input from sensory motor cortex to neostriatum and its modification by conditioning stimulation of the substantia nigra. *Brain Res* 321: 1-8

Huang CY, Rasband MN. 2018. Axon initial segments: structure, function, and disease. *Ann N Y Acad Sci* 1420: 46-61

Ikemoto S. 2007. Dopamine reward circuitry: two projection systems from the ventral midbrain to the nucleus accumbens-olfactory tubercle complex. *Brain Res Rev* 56: 27-78

Jaffe EH, Marty A, Schulte A, Chow RH. 1998. Extrasynaptic vesicular transmitter release from the somata of substantia nigra neurons in rat midbrain slices. *J Neurosci* 18: 3548-53

Kehr W, Carlsson A, Lindqvist M, Magnusson T, Atack C. 1972. Evidence for a receptor-mediated feedback control of striatal tyrosine hydroxylase activity. *J Pharm Pharmacol* 24: 744-7

Keiflin R, Janak PH. 2015. Dopamine Prediction Errors in Reward Learning and Addiction: From Theory to Neural Circuitry. *Neuron* 88: 247-63

Kitai ST, Shepard PD, Callaway JC, Scroggs R. 1999. Afferent modulation of dopamine neuron firing patterns. *Curr Opin Neurobiol* 9: 690-7

Koeltzow TE, Xu M, Cooper DC, Hu XT, Tonegawa S, et al. 1998. Alterations in dopamine release but not dopamine autoreceptor function in dopamine D3 receptor mutant mice. *J Neurosci* 18: 2231-8

Kollins SH, Adcock RA. 2014. ADHD, altered dopamine neurotransmission, and disrupted reinforcement processes: implications for smoking and nicotine dependence. *Prog Neuropsychopharmacol Biol Psychiatry* 52: 70-8

Kosaka T. 1980. The axon initial segment as a synaptic site: ultrastructure and synaptology of the initial segment of the pyramidal cell in the rat hippocampus (CA3 region). *J Neurocytol* 9: 861-82

Lammel S, Hetzel A, Hackel O, Jones I, Liss B, Roeper J. 2008. Unique properties of mesoprefrontal neurons within a dual mesocorticolimbic dopamine system. *Neuron* 57: 760-73

Le Moine C, Bloch B. 1991. Rat striatal and mesencephalic neurons contain the long isoform of the D2 dopamine receptor mRNA. *Brain Res Mol Brain Res* 10: 283-9

Leterrier C. 2016. The Axon Initial Segment, 50 Years Later: A Nexus for Neuronal Organization and Function. *Curr Top Membr* 77: 185-233

Leterrier C. 2018. The Axon Initial Segment: An Updated Viewpoint. *J Neurosci* 38: 2135-45

Leterrier C, Dargent B. 2014. No Pasaran! Role of the axon initial segment in the regulation of protein transport and the maintenance of axonal identity. *Semin Cell Dev Biol* 27: 44-51

Li X, Qi J, Yamaguchi T, Wang HL, Morales M. 2013. Heterogeneous composition of dopamine neurons of the rat A10 region: molecular evidence for diverse signaling properties. *Brain Struct Funct* 218: 1159-76

Liu C, Kershberg L, Wang J, Schneeberger S, Kaeser PS. 2018. Dopamine Secretion Is Mediated by Sparse Active Zone-like Release Sites. *Cell* 172: 706-18 e15

Lohani S, Martig AK, Underhill SM, DeFrancesco A, Roberts MJ, et al. 2018. Burst activation of dopamine neurons produces prolonged post-burst availability of actively released dopamine. *Neuropsychopharmacology* 43: 2083-92

Marcott PF, Mamaligas AA, Ford CP. 2014. Phasic dopamine release drives rapid activation of striatal D2-receptors. *Neuron* 84: 164-76

Martina M, Vida I, Jonas P. 2000. Distal initiation and active propagation of action potentials in interneuron dendrites. *Science* 287: 295-300

Mathiisen TM, Nagelhus EA, BJouleh B, RTorp R, Frydenlund DS, et al. 2006. Postembedding Immunogold Cytochemistry of Membrane Molecules and Amino Acid Transmitters in the Central Nervous System In *Neuroanatomical Tract-Tracing 3: Molecules, Neurons, and Systems*, ed. L Zaborszky, FG Wouterlood, JL Lanciego. New York, NY: Springer Science+Business Media, Inc.

Matsuda W, Furuta T, Nakamura KC, Hioki H, Fujiyama F, et al. 2009. Single nigrostriatal dopaminergic neurons form widely spread and highly dense axonal arborizations in the neostriatum. *J Neurosci* 29: 444-53

McCutcheon RA, Abi-Dargham A, Howes OD. 2019. Schizophrenia, Dopamine and the Striatum: From Biology to Symptoms. *Trends Neurosci* 42: 205-20

Mercuri NB, Saiardi A, Bonci A, Picetti R, Calabresi P, et al. 1997. Loss of autoreceptor function in dopaminergic neurons from dopamine D2 receptor deficient mice. *Neuroscience* 79: 323-7

Meza RC, Lopez-Jury L, Canavier CC, Henny P. 2018. Role of the Axon Initial Segment in the Control of Spontaneous Frequency of Nigral Dopaminergic Neurons In Vivo. *J Neurosci* 38: 733-44

Missale C, Nash SR, Robinson SW, Jaber M, Caron MG. 1998. Dopamine receptors: from structure to function. *Physiol Rev* 78: 189-225

Montague PR, Dayan P, Sejnowski TJ. 1996. A framework for mesencephalic dopamine systems based on predictive Hebbian learning. *J Neurosci* 16: 1936-47

Morelli M, Mennini T, Di Chiara G. 1988. Nigral dopamine autoreceptors are exclusively of the D2 type: quantitative autoradiography of [125I]iodosulpride and [125I]SCH 23982 in adjacent brain sections. *Neuroscience* 27: 865-70

Nair-Roberts RG, Chatelain-Badie SD, Benson E, White-Cooper H, Bolam JP, Ungless MA. 2008. Stereological estimates of dopaminergic, GABAergic and glutamatergic neurons in the ventral tegmental area, substantia nigra and retrorubral field in the rat. *Neuroscience* 152: 1024-31

Nakano T, Yoshimoto J, Doya K. 2013. A model-based prediction of the calcium responses in the striatal synaptic spines depending on the timing of cortical and dopaminergic inputs and post-synaptic spikes. *Front Comput Neurosci* 7: 119

Nemoto C, Hida T, Arai R. 1999. Calretinin and calbindin-D28k in dopaminergic neurons of the rat midbrain: a triple-labeling immunohistochemical study. *Brain Res* 846: 129-36

Nirenberg MJ, Chan J, Liu Y, Edwards RH, Pickel VM. 1996. Ultrastructural localization of the vesicular monoamine transporter-2 in midbrain dopaminergic neurons: potential sites for somatodendritic storage and release of dopamine. *J Neurosci* 16: 4135-45

Paladini CA, Robinson S, Morikawa H, Williams JT, Palmiter RD. 2003. Dopamine controls the firing pattern of dopamine neurons via a network feedback mechanism. *Proc Natl Acad Sci U S A* 100: 2866-71

Paladini CA, Tepper JM. 1999. GABA(A) and GABA(B) antagonists differentially affect the firing pattern of substantia nigra dopaminergic neurons in vivo. *Synapse* 32: 165-76

Peters A, Palay SL, Webster HD. 1991. *The Fine Structure of the Nervous System: Neurons and Their Supporting Cells*. New York, NY: Oxford University Press, Inc. .

Peters A, Proskauer CC, Kaiserman-Abramof IR. 1968. The small pyramidal neuron of the rat cerebral cortex. The axon hillock and initial segment. *J Cell Biol* 39: 604-19

Pickel VM, Chan J, Nirenberg MJ. 2002. Region-specific targeting of dopamine D2-receptors and somatodendritic vesicular monoamine transporter 2 (VMAT2) within ventral tegmental area subdivisions. *Synapse* 45: 113-24

Pickel VM, Towle AC, Joh TH, Chan J. 1988. Gamma-aminobutyric acid in the medial rat nucleus accumbens: ultrastructural localization in neurons receiving monosynaptic input from catecholaminergic afferents. *J Comp Neurol* 272: 1-14

Piper RC, Katzmann DJ. 2007. Biogenesis and function of multivesicular bodies. *Annu Rev Cell Dev Biol* 23: 519-47

Prou D, Gu WJ, Le Crom S, Vincent JD, Salamero J, Vernier P. 2001. Intracellular retention of the two isoforms of the D(2) dopamine receptor promotes endoplasmic reticulum disruption. *J Cell Sci* 114: 3517-27

Ramirez OA, Couve A. 2011. The endoplasmic reticulum and protein trafficking in dendrites and axons. *Trends Cell Biol* 21: 219-27

Rice ME. 2000. Distinct regional differences in dopamine-mediated volume transmission. *Prog Brain Res* 125: 277-90

Rice ME, Cragg SJ. 2008. Dopamine spillover after quantal release: rethinking dopamine transmission in the nigrostriatal pathway. *Brain Res Rev* 58: 303-13

Rice ME, Patel JC. 2015. Somatodendritic dopamine release: recent mechanistic insights. *Philos Trans R Soc Lond B Biol Sci* 370

Robinson BG, Bunzow JR, Grimm JB, Lavis LD, Dudman JT, et al. 2017. Desensitized D2 autoreceptors are resistant to trafficking. *Sci Rep* 7: 4379

Rodriguez M, Gonzalez-Hernandez T. 1999. Electrophysiological and morphological evidence for a GABAergic nigrostriatal pathway. *J Neurosci* 19: 4682-94

Schultz W. 1998. Predictive reward signal of dopamine neurons. *J Neurophysiol* 80: 1-27

Sesack SR. 2010. Functional implications of dopamine D2 receptor localization in relation to glutamate neurons. In *Dopamine Handbook*, ed. LL Iversen, SD Iversen, DS B., A Bjorklund, pp. 22-38. New York, NY: Oxford University Press

Sesack SR, Aoki C, Pickel VM. 1994. Ultrastructural localization of D2 receptor-like immunoreactivity in midbrain dopamine neurons and their striatal targets. *J Neurosci* 14: 88-106

Sesack SR, Grace AA. 2010. Cortico-basal ganglia reward network: microcircuitry. *Neuropsychopharmacology* 35: 27-47

Sesack SR, Miner LH, Omelchenko N. 2006. Preembedding Immunoelectron MIcroscopy: Applications for Studies of the Nervous System In *Neuroanatomical Tract-Tracing 3: Molecules, Neurons, and Systems*, ed. L Zaborszky, FG Wouterlood, JL Lanciego, pp. 6-71. New York, NY: Springer Science+Business Media, Inc.

Shepard PD, Bunney BS. 1988. Effects of apamin on the discharge properties of putative dopamine-containing neurons in vitro. *Brain Res* 463: 380-4

Smith AD, Bolam JP. 1990. The neural network of the basal ganglia as revealed by the study of synaptic connections of identified neurones. *Trends Neurosci* 13: 259-65

Solinas M, Belujon P, Fernagut PO, Jaber M, Thiriet N. 2018. Dopamine and addiction: what have we learned from 40 years of research. *J Neural Transm (Vienna)*

Somogyi P, Tamas G, Lujan R, Buhl EH. 1998. Salient features of synaptic organisation in the cerebral cortex. *Brain Res Brain Res Rev* 26: 113-35

Steinfels GF, Heym J, Jacobs BL. 1981. Single unit activity of dopaminergic neurons in freely moving cats. *Life Sci* 29: 1435-42

Tepper JM, Martin LP, Anderson DR. 1995. GABAA receptor-mediated inhibition of rat substantia nigra dopaminergic neurons by pars reticulata projection neurons. *J Neurosci* 15: 3092-103

Ungless MA, Grace AA. 2012. Are you or aren't you? Challenges associated with physiologically identifying dopamine neurons. *Trends Neurosci* 35: 422-30

van der Kooy D, Coscina DV, Hattori T. 1981. Is there a non-dopaminergic nigrostriatal pathway? *Neuroscience* 6: 345-57

Veznedaroglu E, Milner TA. 1992. Elimination of artifactual labeling of hippocampal mossy fibers seen following pre-embedding immunogold-silver technique by pretreatment with zinc chelator. *Microsc Res Tech* 23: 100-1

Vives F, Mogenson GJ. 1986. Electrophysiological study of the effects of D1 and D2 dopamine antagonists on the interaction of converging inputs from the sensory-motor cortex and substantia nigra neurons in the rat. *Neuroscience* 17: 349-59

Volkow ND, Wise RA, Baler R. 2017. The dopamine motive system: implications for drug and food addiction. *Nat Rev Neurosci* 18: 741-52

Wang H, Pickel VM. 2002. Dopamine D2 receptors are present in prefrontal cortical afferents and their targets in patches of the rat caudate-putamen nucleus. *J Comp Neurol* 442: 392-404

Wang SSH, Held RG, Wong MY, Liu C, Karakhanyan A, Kaeser PS. 2016. Fusion Competent Synaptic Vesicles Persist upon Active Zone Disruption and Loss of Vesicle Docking. *Neuron* 91: 777-91

Watabe-Uchida M, Zhu L, Ogawa SK, Vamanrao A, Uchida N. 2012. Whole-brain mapping of direct inputs to midbrain dopamine neurons. *Neuron* 74: 858-73

Williams J, Lacey M. 1988. Actions of cocaine on central monoamine neurons: intracellular recordings in vitro. *NIDA Res Monogr* 90: 234-42

Wolf ME, Roth RH. 1990. Autoreceptor regulation of dopamine synthesis. *Ann N Y Acad Sci* 604: 323-43

Yang CR, Mogenson GJ. 1984. Electrophysiological responses of neurones in the nucleus accumbens to hippocampal stimulation and the attenuation of the excitatory responses by the mesolimbic dopaminergic system. *Brain Res* 324: 69-84

Yang CR, Mogenson GJ. 1986. Dopamine enhances terminal excitability of hippocampal-accumbens neurons via D2 receptor: role of dopamine in presynaptic inhibition. *J Neurosci* 6: 2470-8

Yang S, Ben-Shalom R, Ahn M, Liptak AT, van Rijn RM, et al. 2016. beta-Arrestin-Dependent Dopaminergic Regulation of Calcium Channel Activity in the Axon Initial Segment. *Cell Rep* 16: 1518-26

Yetnikoff L, Lavezzi HN, Reichard RA, Zahm DS. 2014. An update on the connections of the ventral mesencephalic dopaminergic complex. *Neuroscience* 282: 23-48

Yim CY, Mogenson GJ. 1982. Response of nucleus accumbens neurons to amygdala stimulation and its modification by dopamine. *Brain Res* 239: 401-15

Young B, Wertman J, Dupre DJ. 2015. Regulation of GPCR Anterograde Trafficking by Molecular Chaperones and Motifs. *Prog Mol Biol Transl Sci* 132: 289-305

Yung KK, Bolam JP. 2000. Localization of dopamine D1 and D2 receptors in the rat neostriatum: synaptic interaction with glutamate- and GABA-containing axonal terminals. *Synapse* 38: 413-20

Yung KK, Bolam JP, Smith AD, Hersch SM, Ciliax BJ, Levey AI. 1995. Immunocytochemical localization of D1 and D2 dopamine receptors in the basal ganglia of the rat: light and electron microscopy. *Neuroscience* 65: 709-30

Zahm DS, Root DH. 2017. Review of the cytology and connections of the lateral habenula, an avatar of adaptive behaving. *Pharmacol Biochem Behav* 162: 3-21